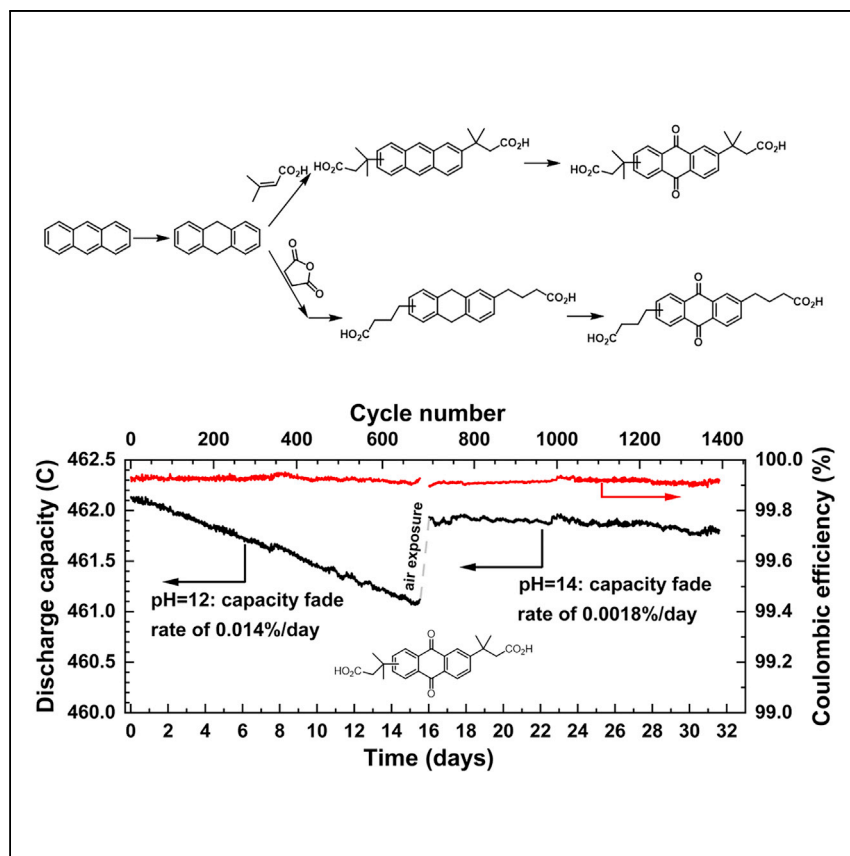


Article

Extremely Stable Anthraquinone Negolytes Synthesized from Common Precursors



Two extremely stable anthraquinone negolytes were synthesized from inexpensive precursors that potentially decrease the mass production cost. The carbon-linked anthraquinones eliminate S_N2 or S_NAr side reactions. Pairing with a $Fe(CN)_6^{3-/4-}$ polysolite, they exhibited an open-circuit voltage of 1.0 V. By operating at pH 14, a record low capacity fade rate of <1% per year was demonstrated.

Min Wu, Yan Jing, Andrew A. Wong, ..., Zhijiang Tang, Roy G. Gordon, Michael J. Aziz

gordon@chemistry.harvard.edu (R.G.G.)
maziz@harvard.edu (M.J.A.)

HIGHLIGHTS

Potentially low-cost and extremely stable anthraquinone negolytes

No S_N2 or S_NAr decomposition reaction in carbon-linked anthraquinones

Record low capacity fade rate of <1% per year

Molecules exhibit longer lifetime at high pH than that at mild pH

Article

Extremely Stable Anthraquinone Negolytes Synthesized from Common Precursors

Min Wu,¹ Yan Jing,² Andrew A. Wong,¹ Eric M. Fell,¹ Shijian Jin,¹ Zhijiang Tang,¹ Roy G. Gordon,^{1,2,*} and Michael J. Aziz^{1,3,*}

SUMMARY

Synthetic cost and long-term stability remain two of the most challenging barriers for the utilization of redox-active organic molecules in redox flow batteries for grid-scale energy storage. Starting from potentially inexpensive 9,10-dihydroanthracene, we developed a new synthetic approach for two extremely stable anthraquinone negolytes, i.e., 3,3'-(9,10-anthraquinone-diyl)bis(3-methylbutanoic acid) (DPivOHAQ) and 4,4'-(9,10-anthraquinone-diyl)dibutanoic acid (DBAQ). Pairing with a ferrocyanide posolyte at pH 12, DPivOHAQ and DBAQ can transfer up to 1.4 and 2 M electrons with capacity fade rates of 0.014% per day and 0.0084% per day, respectively, and exhibit 1.0 V of open-circuit voltage. By adjusting the supporting electrolytes to pH 14, DPivOHAQ exhibited a record low capacity fade rate of <1% per year. We attribute the capacity loss of these flow batteries primarily to the formation of anthrone, which can be suppressed by increasing the pH of the electrolyte and reversed by exposure to air.

INTRODUCTION

The cost of solar and wind electricity has dropped so precipitously that the main barrier to widespread implementation is their intrinsic intermittency.^{1–3} A safe, low-cost, large-scale electrical energy storage system could enable grid-scale adoption of renewables. Among the numerous proposed technologies, redox flow batteries (RFBs) have been recognized as a potentially viable strategy to address the intermittency of renewable energy.^{2–4} Compared with conventional stationary rechargeable batteries (e.g., lithium-ion batteries and lead-acid batteries), RFBs use redox-active materials dissolved in liquid supporting electrolytes that are stored in external tanks and separated from the power generation stack. This separation allows for the decoupling of energy capacity from output power capacity, thereby providing the possibility of low-cost long-duration discharge.^{2–4}

Aqueous RFBs, featuring non-flammable electrolytes, are particularly suitable for storing massive amounts of electricity. Aqueous vanadium RFBs are the most widely studied and adopted systems, but are hindered by the high cost of vanadium.^{3–5} In contrast, redox-active organic molecules comprising earth abundant elements such as carbon (C), hydrogen (H), oxygen (O), and nitrogen (N) have the potential to be inexpensive alternatives to vanadium.^{6–13} Additionally, the structural diversity and tunability of organics enable chemists to design organics with essential properties such as high aqueous solubility, high chemical stability, fast kinetics, and appropriate redox potential.^{6,8–12,14,15}

Recently, water-soluble anthraquinones 4,4'-([9,10-anthraquinone-2,6-diyl]dioxo)di-butyrates (2,6-DBEAQ) and ([9,10-dioxo-9,10-dihydroanthracene-2,6-diyl]bis[oxy])

The Bigger Picture

The cost of solar and wind electricity is decreasing so rapidly that a grid-scale energy storage technology will become essential. Aqueous organic redox flow batteries are a potentially safe, inexpensive substitute for lithium-ion batteries and vanadium flow batteries for large-scale energy storage. Here, we report a new synthetic strategy for two extremely stable anthraquinone negolyte (negative electrolyte) molecules starting from inexpensive precursors that potentially decrease the cost when scaled up. Additionally, we demonstrate that an anthraquinone negolyte is more stable running at pH 14 than at pH 12, and is expected to be more stable in alkaline solution than in acidic or neutral conditions. Paired with a $\text{Fe}(\text{CN})_6^{3-/4-}$ positive electrolyte, the anthraquinone cell exhibited a record low capacity fade rate of <1% per year. The new synthetic strategy for these highly stable anthraquinone negolytes might facilitate the commercialization of anthraquinone-based flow batteries.

bis[propane-3,1-diyl]bis(phosphonic acid) (2,6-DPPEAQ) in mildly alkaline solutions have demonstrated extremely low temporal fade rates in flow batteries paired with $K_4Fe(CN)_6$.^{16–18} These quinones are chemically synthesized from 2,6-dihydroxyanthraquinone (2,6-DHAQ) by industry-compatible methods. However, 2,6-DHAQ and 2,7-DHAQ are always co-produced and are costly to separate. Furthermore, our previous research showed that the molecular lifetimes of anthraquinone-based electrolytes can differ by two orders of magnitude depending on the positions of their functional groups (e.g., 1,8- and 2,6-anthraquinones).^{16,19} Therefore, it is important to quantify the stabilities of organic molecules with a mixture of isomers. Additionally, 2,6-DHAQ and 2,7-DHAQ are synthesized from 9,10-anthraquinone-2,6-disulfonic acid and 9,10-anthraquinone-2,7-disulfonic acid, respectively, in strong alkaline solution for 35 h at a high temperature (180 °C) with a moderate yield, which is energy-intensive and costly.²⁰ Thus, designing low-cost and chemically stable anthraquinones is of vital importance for the commercialization of aqueous organic RFBs.

Because of the inherent chemical stability of the parent structure, the addition of side chains to an anthraquinone core is usually accomplished by a stepwise procedure via anthraquinone derivatives (e.g., hydroxylated anthraquinone or chlorinated anthraquinone).^{16,17,19,21} Here, we report a new synthetic route for water-soluble anthraquinones starting from a potentially inexpensive anthracene derivative, 9,10-dihydroanthracene, which can be readily produced from anthracene with a yield of almost 100%.^{22,23} Anthracene, a component of coal tar, is one of the major resources for large-scale anthraquinone production.²⁴ The first step is a Friedel-Crafts alkylation or acylation to render dihydroanthracene and anthracene water-soluble; the last step is an oxidation to produce the corresponding redox-active anthraquinones, i.e., 3,3'-(9,10-anthraquinone-diyl)bis(3-methylbutanoic acid) (DPivOHAQ) and 4,4'-(9,10-anthraquinone-diyl)dibutanoic acid (DBAQ).

Both molecules exhibit high water solubility and chemical stability at pH 12. The DBAQ negolyte (negative electrolyte) has a water solubility of 1.0 M, corresponding to a volumetric capacity of 53.6 Ah L⁻¹; when paired with potassium ferrocyanide, a full cell exhibited a capacity fade rate of 0.0084% per day or 3.1% per year. DPivOHAQ has a solubility of 0.74 M; when paired with potassium ferrocyanide, a full cell exhibited a capacity fade rate of 0.014% per day or 5.1% per year. Additionally, we demonstrated that the DPivOHAQ negolyte is even more stable in strong base, exhibiting a capacity fade rate of 0.0018% per day or 0.66% per year at pH 14. Furthermore, we demonstrated that the capacity fade is due to formation of anthrone, which can convert back to anthraquinone through air exposure and can also be suppressed at high pH. Thus, these findings suggest that, through a combination of increased pH and periodic air exposure, both DPivOHAQ and DBAQ offer the possibility of decadal lifetimes in aqueous RFBs. In the following section we report methods and results, first for DPivOHAQ and then for DBAQ.

RESULTS AND DISCUSSION

Figure 1 illustrates the synthetic routes, chemical structure, Pourbaix diagram, and cyclic voltammogram (CV) of DPivOHAQ. Synthesis was achieved by first functionalizing 9,10-dihydroanthracene with the water-soluble group $-C(CH_3)_2CH_2COOH$, followed by an oxidation step with CrO_3 . The oxidation step is well known in industry for anthraquinone synthesis, and it can also be accomplished by other methods, such as nitric acid and air, as confirmed by the ¹H NMR of DPivOHAQ in Figure S3, that could further decrease the costs when scaled up.^{25,26} However, CrO_3 oxidation

¹John A. Paulson School of Engineering and Applied Sciences, Harvard University, Cambridge, MA 02138, USA

²Department of Chemistry and Chemical Biology, Harvard University, Cambridge, MA 02138, USA

³Lead Contact

*Correspondence: gordon@chemistry.harvard.edu (R.G.G.), maziz@harvard.edu (M.J.A.)

<https://doi.org/10.1016/j.chempr.2020.03.021>

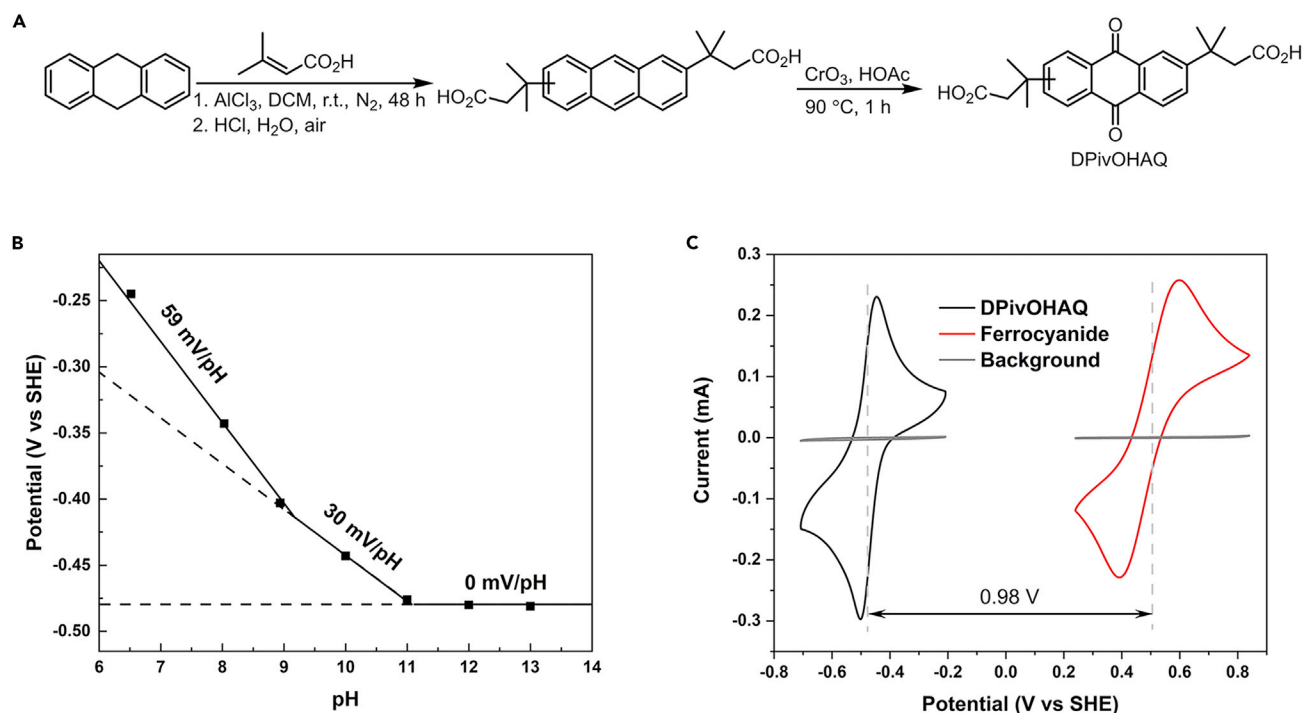


Figure 1. DPivOHAQ Synthesis and Electrochemistry

(A) Synthetic route for DPivOHAQ.

(B) Pourbaix diagram.

(C) Cyclic voltammograms of 5 mM DPivOHAQ and 10 mM potassium ferrocyanide at pH 12 with a scan rate of 100 mV s⁻¹.

is a more controllable method on a research scale to get a purer product, therefore, in this work, we use CrO₃ as the oxidant unless specifically mentioned otherwise. Compared with 2,6-DBEAQ and 2,6-DPPEAQ synthesis, the reported synthetic approach could be potentially more cost-effective. For example, assuming anthracene is the starting material, both DBEAQ and DPPEAQ require five synthetic steps in total as illustrated in [Scheme S1](#) with an overall yield around 52% and 59%, respectively; whereas, DPivOHAQ synthesis requires only three steps with an overall yield of 81%. Moreover, the cost of side chains for DPivOHAQ is slightly lower than that of DBEAQ and substantially lower than that of DPPEAQ at sub-kg scales, as shown in [Table S1](#). Therefore, we expect that DPivOHAQ is most likely less expensive to produce than DBEAQ and DPPEAQ at industrial scales.

In addition to potentially lower synthetic costs, DPivOHAQ is functionalized with carbon-linked functional groups, which are chemically more robust than the oxygen-linked side chains in DBEAQ and DPPEAQ, minimizing the opportunity for S_N2 and S_NAr side reactions to occur.^{16,17} The thermochemical stability of both oxidized and reduced forms of DPivOHAQ were evaluated at high temperature (65 °C) and in strongly alkaline conditions (pH 14) for eight days. No apparent decomposition was detected from the ¹H NMR as shown in [Figure S8](#), indicating that DPivOHAQ is quite chemically stable. A temperature of 65 °C is well above anticipated operating temperatures of RFBs; thus there should be much less decomposition in real applications.

Synthesis of DPivOHAQ results in a mixture of 2,6- and 2,7- isomers that does not require further separation prior to use in a battery. The Pourbaix diagram of DPivOHAQ, shown in [Figure 1B](#), suggests that the molecule undergoes a two-proton/

two-electron process below pH 9, a one-proton/two-electron process between pH 9 and 11, and a zero-proton process with a pH-independent potential of approximately -0.48 V versus standard hydrogen electrode (SHE) at pH > 11 . Pairing a DPi-vOHAQ negolyte with potassium ferrocyanide at pH 12 should yield an equilibrium cell potential of approximately 0.98 V (Figure 1C). Electrochemical kinetics of DPi-vOHAQ reduction were determined with the rotating disk electrode (RDE) method as shown in Figure S9. The charge transfer coefficient is 0.49 , the diffusion coefficient is 2.4×10^{-6} cm² s⁻¹, and the kinetic rate constant is 2.5×10^{-3} cm s⁻¹; the latter is much higher than is typical of inorganic redox-active materials at an uncatalyzed carbon electrode.²⁷ It should be noted that such a high kinetic rate constant could be a lower bound to the actual value, because a RDE system exhibits mixed kinetic and transport limits in the observed mass-transfer limited current density region. The solubilities of the oxidized forms of anthraquinones in alkaline solutions are typically lower than those of the reduced forms. The solubility of DPi-vOHAQ at pH 12 was determined by UV-vis spectrophotometry (Figure S10) to be 0.74 M, corresponding to a volumetric capacity of 39.7 Ah L⁻¹.

Polarization experiments of a 0.5 M DPi-vOHAQ-ferrocyanide full cell at pH 12 were performed at various states of charge. The electrolytes comprised 5 mL of 0.5 M DPi-vOHAQ (negolyte) at pH 12 (10 mM KOH) and 80 mL of 0.3 M potassium ferrocyanide and 0.1 M potassium ferricyanide (posolyte) at pH 12. The cell was constructed from graphite flow plates and AvCarb carbon cloth electrodes, separated by a Fuma-sep E-620 (K) membrane because of its low permeability to ferricyanide and high ionic conductivity.^{16,17} A peak galvanic power density of 0.34 W cm⁻² was achieved at $\sim 100\%$ state of charge (SOC) (Figure 2A). Careful attention to engineering design and construction should raise the power density even farther.²⁸ The open-circuit voltage (OCV) increases from 0.95 to 1.08 V as the SOC increases from 10% to $\sim 100\%$, and the OCV at 50% SOC of 0.99 V (Figure 2B) is consistent with the voltage expected from CV. The alternating current area-specific resistance (ASR) of the cell was determined via high-frequency potentiostatic electrochemical impedance spectroscopy (EIS), and the value was below 0.6 Ω cm² across all SOC (Figure 2B). This is a relatively low alternating current ASR value for RFBs with alkaline electrolytes.^{16,17} The polarization ASR was determined using the linear region within the voltage range 0.9 – 1.1 V (Figures 2A and 2B). The ASR of the membrane (0.54 Ω cm² at 50% SOC, determined by high-frequency EIS in the full cell) accounted for around 67% of the ASR of the entire cell (0.81 Ω cm² at 50% SOC, DC polarization). The capacity utilization for the negolyte (capacity-limiting side) is approximately 95% at 50 mA cm⁻² with a high round-trip energy efficiency of 91.5% (Figures 2C and 2D). At a reasonable practical operation target of 80% round-trip energy efficiency, the low value of the ASR permits galvanostatic operation at around 140 mA cm⁻² with an electrolytic power density of 0.16 W cm⁻², a galvanic power density of 0.13 W cm⁻², and 92% capacity utilization.

The same 0.5 M DPi-vOHAQ-ferrocyanide full cell was used for long-term stability evaluation (Figure 3). The cell was cycled at a constant current density of ± 0.1 A cm⁻², and each galvanostatic half cycle was followed by a potential hold at the voltage limit (1.3 V for charge, 0.6 V for discharge) until the current density fell below 2 mA cm⁻² to mitigate the effect of temporal variations in accessible capacity during full cell cycling caused by drifts in cell resistance.²⁹ The charge-discharge profiles near the voltage limits (Figures 3B and 3C) are quite steep and are followed by small subsequent horizontal segments during the potential holds. The horizontal segments end at 95.5% of theoretical capacity of negolyte, but the steepness followed by a small subsequent horizontal segment of the charge-discharge profiles suggests

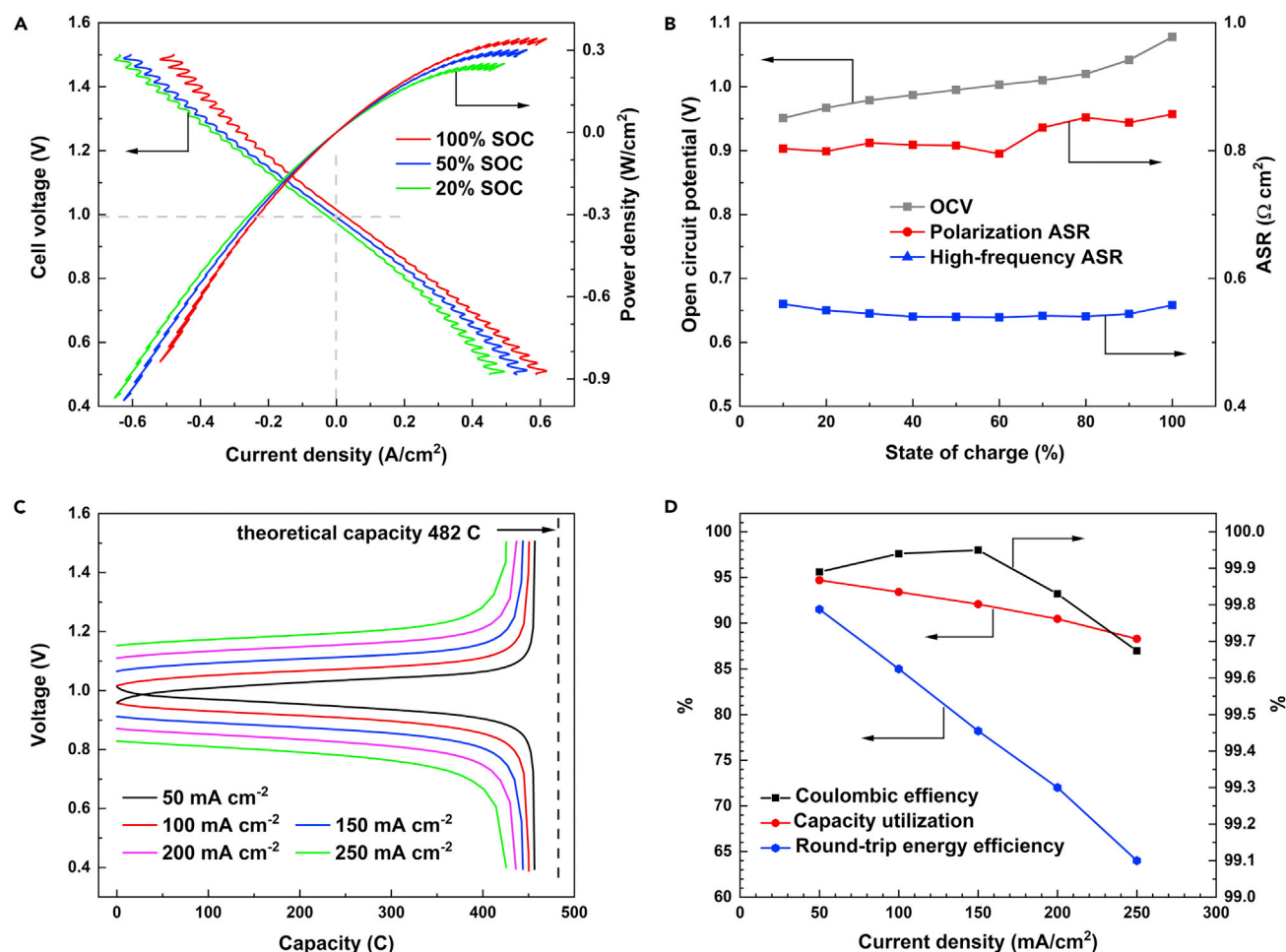


Figure 2. Polarization Measurements of 0.5 M DPivOHAQ/Ferrocyanide Full Cell at pH 12

(A) Cell voltage versus current density at room temperature ($\sim 20^\circ\text{C}$) at various SOC.

(B) OCV, high-frequency ASR and polarization ASR versus SOC.

(C) Galvanostatic charge-discharge voltage profiles at various current densities. The vertical dashed line indicates the theoretical capacity.

(D) Capacity utilization, Coulombic efficiency, and round-trip energy efficiency versus current density.

that the electrolyte had around 4.5% inactive material and that the active material is undergoing deep cycling to essentially the full SOC limits. The cell was cycled for 690 cycles at 100 mA cm^{-2} , which required 15.6 days to complete. The capacity retention over the 690 cycles was 99.78% with an average Coulombic efficiency greater than 99.9%, reflecting a capacity fade rate of 0.00031% per cycle or 0.014% per day (Figure 3A), i.e., 5.1% per year. This temporal fade rate is among the lowest exhibited by full cells in which organic molecules composed the capacity-limiting side: 2,6-DBEAQ fades at $\sim 0.04\%$ per day; 2,6-DPPEAQ fades at $\sim 0.014\%$ per day.¹⁸

After 15.6 days of cycling at pH 12, DPivOHAQ negolyte, in the discharged state, was exposed to air for 2 h and the pH was adjusted to 14 by dissolving KOH pellets into the negolyte and posolyte without changing cell materials or setup. As a result, 81% of the lost capacity was recovered, as shown in Figure 3A. Over the additional 16 days at pH 14, the cell exhibited a capacity fade rate of 0.0018% per day, which is 6 times lower than that at pH 12. The charge-discharge voltage profiles (Figures 3B and 3C) are almost invariant, indicating no apparent change in ohmic resistance and

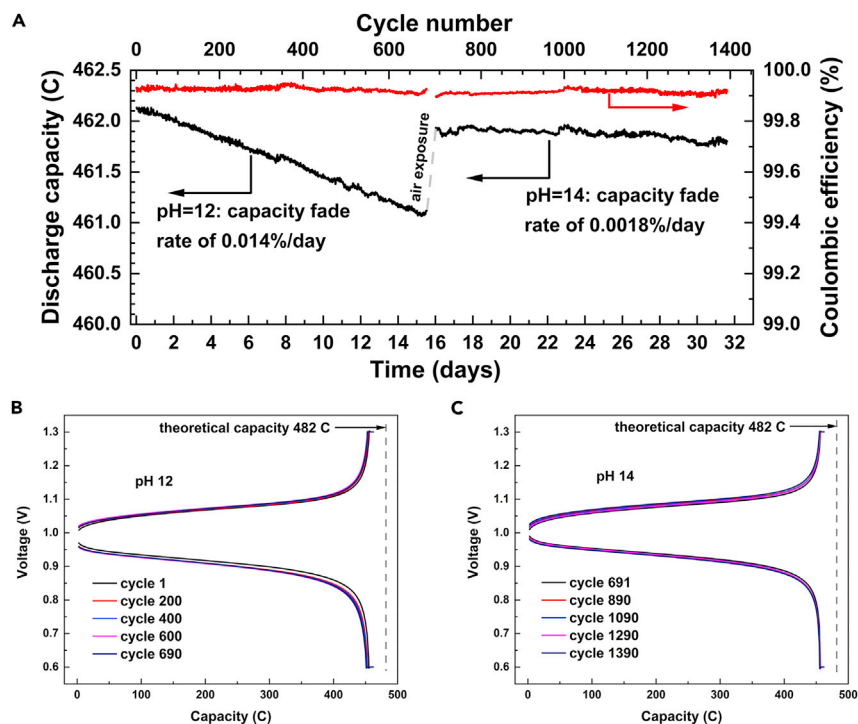


Figure 3. Cycling Performance of DPivOHAQ at pH 12 and 14

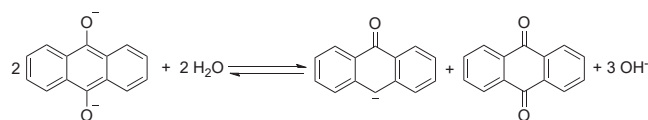
(A) Coulombic efficiency and discharge capacity versus time and cycle number for a negolyte-limited DPivOHAQ/ $\text{K}_4\text{Fe}(\text{CN})_6$ full cell. Each 100 mA cm^{-2} half cycle was followed by a potentiostatic hold until the magnitude of the current density fell below 2 mA cm^{-2} . The negolyte comprised 5 mL of 0.5 M DPivOHAQ at pH 12, and the posolyte comprised 80 mL of 0.3 M potassium ferrocyanide and 0.1 M potassium ferricyanide at pH 12. After approximately 16 days of cycling, the negolyte was exposed to air and the pH of both negolyte and posolyte were adjusted to 14 before cycling for an additional 16 days. Note that the left y axis represents only 0.54% of the capacity of the DPivOHAQ negolyte.

(B) Charge-discharge voltage profile of DPivOHAQ from selected cycles at pH 12 in Figure 3A.

(C) Charge-discharge voltage profile of DPivOHAQ from selected cycles at pH 14 in Figure 3A.

good chemical compatibility with cell membrane and other cell components.³⁰ Based on the decomposition study of 2,6-DHAQ,³¹ we attribute capacity fade to anthrone formation (Scheme 1). Therefore, increasing the hydroxide concentration should suppress the formation of anthrone. This expectation is consistent with the lower capacity fade rate observed at pH 14 than at pH 12. In general, the disproportionation reaction will generate OH^- (or consume H^+) at pH above the first pK_a of the anthrahydroquinone. Therefore, anthrone formation will be disfavored under alkaline conditions relative to acid conditions and will be progressively disfavored as the pH increases (Figure S11). We interpret the sudden increase in capacity at cycle 691 as the consequence of anthrone being converted back to anthraquinone by both the pH effect and the effect of exposure to atmospheric O_2 .

To confirm the major side reaction is the disproportionation of reduced anthraquinone, a fully reduced ($\sim 100\%$ SOC) sample of DPivOHAQ at pH 12 was prepared and stored in a fluorinated ethylene propylene (FEP) vial in a glove box for 238 days, allowing the disproportionation to reach equilibrium. Indeed, some appreciable side peaks appeared in the ^1H NMR spectrum of the reduced DPivOHAQ, whereas upon re-oxidation in air, the ^1H NMR spectrum contained no observable decomposition peaks (Figure S12), indicating that the decomposition compounds can either be re-oxidized back to



Scheme 1. The Reversible Disproportionation Reaction of Anthraquinone Negolyte under Alkaline Conditions

The pK_a of anthrone is reported³² to be 10; therefore, anthrone is depicted in the deprotonated form at pH values between 12 and 14.³¹

DPivOHAQ or are converted to other products with no observable signals above the detection limit of the NMR instrument. Therefore, high-performance liquid chromatography-mass spectrometry was performed to analyze both the reduced and the re-oxidized samples (Figure S13). The anthrone species was detected in the reduced sample but not in the re-oxidized sample, in agreement with the ^1H NMR result shown in Figure S12. In the re-oxidized sample after 238 days, approximately 1.24% of the signal corresponded to an anthrone dimer, suggesting a fade rate of 1.90% per year for reduced DPivOHAQ at pH 12 after aeration.

Goulet et al. showed that, by avoiding high SOC, the anthrone formation rate in 2,6-DHAQ decreased substantially.³¹ They also demonstrated recovery of most of the lost capacity by air exposure. Because DPivOHAQ also decomposes via anthrone formation, we hypothesize that similar approaches will extend its lifetime significantly. We suggest that a flow cell with decades-long calendar life might be achievable with DPivOHAQ at pH 12.

Another anthraquinone, DBAQ, with higher solubility, was synthesized (Figure 4A) using a similar strategy. The first step is a Friedel-Crafts acylation, followed by Wolff-Kishner reduction of the carbonyl groups to methylene. The last step is to oxidize the corresponding anthracene (or 9,10-dihydroanthracene) to the final anthraquinone form. Compared with the three steps for DPivOHAQ synthesis, four steps are required for DBAQ synthesis when starting from anthracene. Because of the low cost of succinic anhydride and given that the Wolff-Kishner reduction is well-developed in industry, the cost of DBAQ could also be low. Electrochemical kinetics studies of DBAQ were conducted by RDE techniques as shown in Figure S14A. The diffusion coefficient of the oxidized form of DBAQ was determined by Levich analysis (Figure S14B) to be $2.5 \times 10^{-6} \text{ cm}^2 \text{ s}^{-1}$. According to the Koutecký-Levich equation and Tafel plot, the charge transfer coefficient is 0.50, and the kinetic rate constant is $2.9 \times 10^{-3} \text{ cm s}^{-1}$, which is still slightly higher than that of DPivOHAQ.

The solubility of DBAQ was determined to be 1.0 M at pH 12, corresponding to a volumetric capacity of 53.6 Ah L^{-1} for the negolyte. The reduction potential is -0.47 V versus SHE at pH 12. When paired with potassium ferrocyanide, a full cell of approximately 0.97 V can be achieved. To evaluate the stability of a DBAQ negolyte, a full cell was assembled with 5 mL of 0.5 M DBAQ negolyte at pH 12 as the capacity-limiting side and a posolyte comprising 80 mL of 0.3 M $\text{K}_4\text{Fe}(\text{CN})_6$ with 0.1 M $\text{K}_3\text{Fe}(\text{CN})_6$ at pH 12 as the non-capacity-limiting side. The flow cell was constructed from graphite flow plates and carbon paper electrodes, separated by a Fumasep E-620 (K) membrane. The cell exhibited 91.7% of its theoretical capacity for the negolyte. It was cycled for 650 cycles at 100 mA cm^{-2} , which required 15.5 days to complete. The average capacity fade rate was 0.0084% per day, corresponding to 3.1% per year. Assuming the capacity fade is primarily due to anthrone formation then, with careful control of the pH and SOC of the DBAQ electrolyte and periodic exposure to air, DBAQ might exhibit an even lower loss rate in real-world applications.

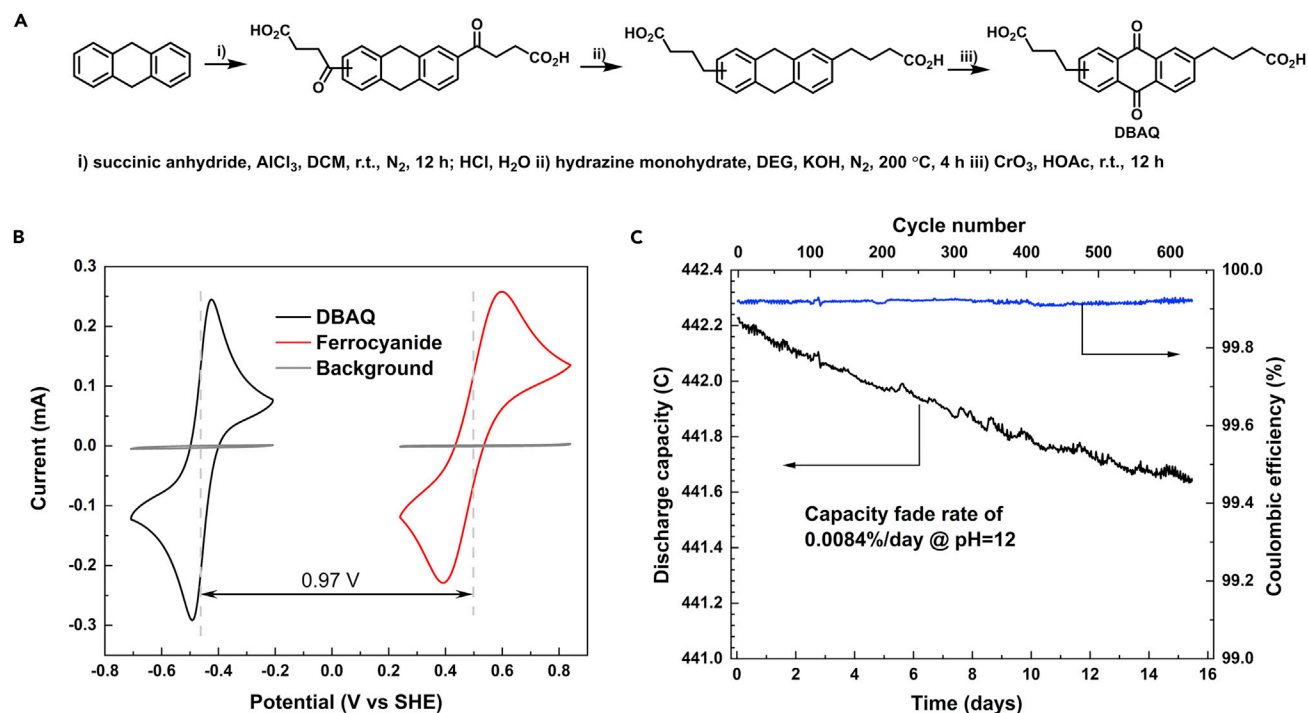


Figure 4. DBAQ Synthesis and Electrochemistry

(A) Synthetic route for DBAQ.

(B) Cyclic voltammograms of 5 mM DBAQ and 10 mM potassium ferrocyanide at pH 12 with a scan rate of 100 mV s^{-1} .

(C) Coulombic efficiency and discharge capacity versus time and cycle number for a negolyte-limited DBAQ/ $\text{K}_4\text{Fe}(\text{CN})_6$ full cell. The cell was cycled galvanostatically at 100 mA cm^{-2} between 0.4 and 1.3 V with SGL 39AA carbon electrodes, and each half cycle was followed by a potentiostatic hold until the magnitude of the current density fell below 2 mA cm^{-2} . The negolyte comprised 5 mL of 0.5 M DBAQ at pH 12, and the posolyte comprised 80 mL of 0.3 M potassium ferrocyanide and 0.1 M potassium ferricyanide at pH 12. Note that the left y axis represents only 0.32% of the capacity of the DBAQ negolyte.

Conclusions

In this report, we have demonstrated a new route to synthesize water-soluble anthraquinones with solubilizing groups attached by carbon-carbon bonds, starting from potentially inexpensive 9,10-dihydroanthracene. These anthraquinones exhibit high aqueous solubilities and low capacity fade rates of 0.0084% per day and 0.014% per day at pH 12, respectively. We demonstrated in a full cell containing a DPivOHAQ negolyte that anthrone formation is the major side reaction responsible for capacity fade and that air exposure can recover most of the lost capacity. Furthermore, by increasing the pH of the negolyte, we demonstrated the suppression of the DPivOHAQ capacity fade rate to an extremely low value of less than 1% per year. We expect that the stability of DPivOHAQ and DBAQ can be even further improved with careful control of the battery operating conditions. We suggest that strategies combining SOC limit control, precision air exposure, and pH tuning can be extended to other inexpensive anthraquinone molecules to achieve extremely low capacity fade rates, paving the way for commercializing anthraquinone-based RFBs to enable grid-scale energy storage of renewable electricity.

EXPERIMENTAL PROCEDURES

Experiment Materials

9,10-dihydroanthracene (97%), 3,3-dimethylacrylic acid (97%), and anhydrous dichloromethane were purchased from Sigma Aldrich. Anhydrous aluminum chloride (95%) was purchased from Alfa Aesar. All chemicals were used as received.

3,3'-(Anthracene-Diyl)Bis(3-Methylbutanoic Acid) (DPivOHAC)

13.32 g (99.93 mmol) of AlCl_3 was suspended in ~ 200 mL of anhydrous CH_2Cl_2 . A solution of 6.67 g (66.62 mmol) of 3,3-dimethylacrylic acid in ~ 20 mL of anhydrous CH_2Cl_2 was added by syringe and the mixture stirred at room temperature ($\sim 20^\circ\text{C}$) for 0.5 h under nitrogen. Subsequently, a solution of 5.00 g (27.74 mmol) of 9,10-dihydroanthracene in ~ 15 mL of anhydrous CH_2Cl_2 was added to the above mixture and stirred for 48 h at room temperature ($\sim 20^\circ\text{C}$). After that, the solvent was quenched with 200 mL of 1 M aqueous HCl and stirred overnight. The organic layer was then removed and the remaining solution was filtered to afford the pale-yellow product. The yield given was 95%.

3,3'-(9,10-Anthraquinone-Diyl)Bis(3-Methylbutanoic Acid) (DPivOHAQ)

DPivOHAC (6.00 g, 15.85 mM) was dissolved in glacial acetic acid (70 mL). Then, a CrO_3 solution (3.33 g, 33.3 mM) was added to the DPivOHAC and acetic acid mixture. The reaction mixture was heated at 90°C for 1 h. After cooling down to room temperature ($\sim 20^\circ\text{C}$), water was added to precipitate the solid. The compound was purified by dissolution in base followed by addition of acid to afford the precipitate. The yield given was 85%.

The ^1H NMR spectra of 3,3'-(anthracene-diyl)bis(3-methylbutanoic acid) and 3,3'-(9,10-anthraquinone-diyl)bis(3-methylbutanoic acid) are shown in Figures S1 and S2. DBAQ-related synthesis uses a similar method, thus is provided in the supporting information.

Full Cell Measurements

Flow battery experiments were conducted with cell hardware from Fuel Cell Tech. (Albuquerque, NM), assembled into a zero-gap flow cell configuration, similar to a previous report.^{17,18} Pyrosealed POCO graphite flow plates with serpentine flow patterns were used for both electrodes. Each electrode comprised a 5 cm^2 geometric surface area covered by one sheet of AvCarb carbon cloth or three sheets of SGL 39AA electrode. For DPivOHAQ-ferrocyanide full cell tests, a Fumasep E-620 (K) membrane was used to serve as the ion-selective membrane between the AvCarb electrodes. For DBAQ-ferrocyanide full cell tests, a Fumasep E-620 (K) membrane was used to serve as the ion-selective membrane between the SGL 39AA electrodes. The outer portion of the space between the electrodes was gasketed by Viton sheets with the area over the electrodes cut out. Torque applied during cell assembly was 60 lb-in (6.78 N m) on each of eight bolts. The electrolytes were fed into the cell through fluorinated ethylene propylene (FEP) tubing at a rate of 60 mL/min, controlled by Cole-Parmer six Masterflex L/S peristaltic pumps. All cells were run inside a nitrogen-filled glove bag. Cell polarization measurements, impedance spectroscopy, and charge-discharge cycling were performed using a Biologic BCS-815 battery cycler. Galvanostatic cycling was performed at $\pm 0.1\text{ A cm}^{-2}$ at room temperature ($\sim 20^\circ\text{C}$) with voltage limits of 0.6 and 1.3 V. To obtain the polarization curves, the cell was first charged to the desired SOC and then polarized via linear sweep voltammetry at a rate of 100 mV s^{-1} . This method was found to yield polarization curves very close to point-by-point galvanostatic holds, yet to impose minimal perturbation to the SOC of the small-electrolyte-volume cell. EIS was performed at SOC between 10% and 100% at open-circuit potential with a 10-mV perturbation and with frequency ranging from 1 to 300,000 Hz.

SUPPLEMENTAL INFORMATION

Supplemental Information can be found online at <https://doi.org/10.1016/j.chempr.2020.03.021>.

ACKNOWLEDGMENTS

This research was supported by U.S. DOE award DE-AC05-76RL01830 through PNNL subcontract 428977, Innovation Fund Denmark via the Grand Solutions project "ORBATS" file number. 7046-00018B, and NSF grant CBET-1914543. The authors thank Daniel A. Pollack for valuable discussions and for assistance with chemical stability experiments and in reviewing and editing the manuscript.

AUTHOR CONTRIBUTIONS

M.W. designed and synthesized the molecules. M.W. conducted the chemical stability and solubility tests, and M.W., A.A.W., Z.T., and Y.J. performed full cell tests. Y.J. also conducted DPivOHAQ synthesis. Y.J. and S.J. identified the anthrone side product and performed HPLC tests. E.M.F. performed the RDE test. R.G.G. supervised the molecular synthesis and characterization. M.J.A. supervised the cell assembly, electrolyte composition selection, and performance evaluation. M.W. drafted the manuscript with input from Y.J. All authors reviewed and edited the manuscript.

DECLARATION OF INTERESTS

Harvard University has filed a patent application on the materials described in this paper.

Received: January 22, 2020

Revised: March 14, 2020

Accepted: March 23, 2020

Published: April 17, 2020

REFERENCES

1. Dunn, B., Kamath, H., and Tarascon, J.M. (2011). Electrical energy storage for the grid: a battery of choices. *Science* 334, 928–935.
2. Yang, Z., Zhang, J., Kintner-Meyer, M.C., Lu, X., Choi, D., Lemmon, J.P., and Liu, J. (2011). Electrochemical energy storage for green grid. *Chem. Rev.* 111, 3577–3613.
3. Soloveichik, G.L. (2015). Flow batteries: current status and trends. *Chem. Rev.* 115, 11533–11558.
4. Darling, R.M., Gallagher, K.G., Kowalski, J.A., Ha, S., and Brushett, F.R. (2014). Pathways to low-cost electrochemical energy storage: a comparison of aqueous and nonaqueous flow batteries. *Energy Environ. Sci.* 7, 3459–3477.
5. Li, L., Kim, S., Wang, W., Vijayakumar, M., Nie, Z., Chen, B., Zhang, J., Xia, G., Hu, J., Graff, G., et al. (2011). A stable vanadium redox-flow battery with high energy density for large-scale energy storage. *Adv. Energy Mater.* 1, 394–400.
6. Huskinson, B., Marshak, M.P., Suh, C., Er, S., Gerhardt, M.R., Galvin, C.J., Chen, X., Aspuru-Guzik, A., Gordon, R.G., and Aziz, M.J. (2014). A metal-free organic-inorganic aqueous flow battery. *Nature* 505, 195–198.
7. Yang, B., Hoober-Burkhardt, L., Wang, F., Surya Prakash, G.K., and Narayanan, S.R. (2014). An inexpensive aqueous flow battery for large-scale electrical energy storage based on water-soluble organic redox couples. *J. Electrochem. Soc.* 161, A1371–A1380.
8. Lin, K., Chen, Q., Gerhardt, M.R., Tong, L., Kim, S.B., Eisenach, L., Valle, A.W., Hardee, D., Gordon, R.G., Aziz, M.J., and Marshak, M.P. (2015). Alkaline quinone flow battery. *Science* 349, 1529–1532.
9. Lin, K., Gómez-Bombarelli, R., Beh, E.S., Tong, L., Chen, Q., Valle, A., Aspuru-Guzik, A., Aziz, M.J., and Gordon, R.G. (2016). A redox-flow battery with an alloxazine-based organic electrolyte. *Nat. Energy* 1, 16102.
10. Beh, E.S., De Porcellinis, D., Gracia, R.L., Xia, K.T., Gordon, R.G., and Aziz, M.J. (2017). A neutral pH aqueous organic-organometallic redox flow battery with extremely high capacity retention. *ACS Energy Lett.* 2, 639–644.
11. Yang, Z., Tong, L., Tabor, D.P., Beh, E.S., Goulet, M.-A., De Porcellinis, D., Aspuru-Guzik, A., Gordon, R.G., and Aziz, M.J. (2018). Alkaline benzoquinone aqueous flow battery for large-scale storage of electrical energy. *Adv. Energy Mater.* 8, 1702056.
12. Hollas, A., Wei, X., Murugesan, V., Nie, Z., Li, B., Reed, D., Liu, J., Sprenkle, V., and Wang, W. (2018). A biomimetic high-capacity phenazine-based anolyte for aqueous organic redox flow batteries. *Nat. Energy* 3, 508–514.
13. Leung, P., Shah, A.A., Sanz, L., Flox, C., Morante, J.R., Xu, Q., Mohamed, M.R., Ponce de León, C., and Walsh, F.C. (2017). Recent developments in organic redox flow batteries: a critical review. *J. Power Sources* 360, 243–283.
14. DeBruler, C., Hu, B., Moss, J., Liu, X., Luo, J., Sun, Y., and Liu, T.L. (2017). Designer two-electron storage viologen anolyte materials for neutral aqueous organic redox flow batteries. *Chem* 3, 961–978.
15. Hu, B., DeBruler, C., Rhodes, Z., and Liu, T.L. (2017). Long-cycling aqueous organic redox flow battery (AORFB) toward sustainable and safe energy storage. *J. Am. Chem. Soc.* 139, 1207–1214.
16. Kwabi, D.G., Lin, K., Ji, Y., Kerr, E.F., Goulet, M.-A., De Porcellinis, D., Tabor, D.P., Pollack, D.A., Aspuru-Guzik, A., Gordon, R.G., and Aziz, M.J. (2018). Alkaline quinone flow battery with long lifetime at pH 12. *Joule* 2, 1894–1906.
17. Ji, Y., Goulet, M.-A., Pollack, D.A., Kwabi, D.G., Jin, S., Porcellinis, D., Kerr, E.F., Gordon, R.G., and Aziz, M.J. (2019). A phosphonate-functionalized quinone redox flow battery at near-neutral pH with record capacity retention rate. *Adv. Energy Mater.* 9, 1900039.
18. Kwabi, D.G., Ji, Y., and Aziz, M.J. (2020). Electrolyte lifetime in aqueous organic redox flow batteries: a critical review. *Chem. Rev.* <https://doi.org/10.1021/acs.chemrev.9b00599>.
19. Jin, S., Jing, Y., Kwabi, D.G., Ji, Y., Tong, L., De Porcellinis, D., Goulet, M.-A., Pollack, D.A., Gordon, R.G., and Aziz, M.J. (2019). A water-miscible quinone flow battery with high volumetric capacity and energy density. *ACS Energy Lett.* 4, 1342–1348.
20. Hall, J., and Perkin, A.G. (1923). CCXXIV.—reduction products of the

- hydroxyanthraquinones. part II. *J. Chem. Soc. Trans.* 123, 2029–2037.
21. Shimizu, A., Takenaka, K., Handa, N., Nokami, T., Itoh, T., and Yoshida, J.I. (2017). Liquid quinones for solvent-free redox flow batteries. *Adv. Mater.* 29, 1606592.
22. Kuimov, V.A., Gusarova, N.K., Malysheva, S.F., and Trofimov, B.A. (2018). Transition metal-free regioselective access to 9,10-dihydroanthracenes via the reaction of anthracenes with elemental phosphorus in the KOH/DMSO system. *Tetrahedron Lett.* 59, 4533–4536.
23. von Grotthuss, E., Prey, S.E., Bolte, M., Lerner, H.W., and Wagner, M. (2019). Dual role of doubly reduced arylboranes as dihydrogen- and hydride-transfer catalysts. *J. Am. Chem. Soc.* 141, 6082–6091.
24. Dieterich, V., Milshtein, J.D., Barton, J.L., Carney, T.J., Darling, R.M., and Brushett, F.R. (2018). Estimating the cost of organic battery active materials: a case study on anthraquinone disulfonic acid. *Transl. Mater. Res.* 5, 034001.
25. Das, C.K., and Das, N.S. (1982). Oxidation of anthracene to anthraquinone in liquid-phase with an air/oxygen/nitric acid system. *J. Chem. Tech. Bioelectron.* 32, 643–649.
26. Rodríguez, F., Blanco, M.D., Adrados, L.F., Burillo, J., and Tijero, J.F. (1989). Selective oxidation of anthracene to anthraquinone in acetic acid with air in presence of nitric acid. *Tetrahedron Lett.* 30, 2417–2420.
27. Weber, A.Z., Mench, M.M., Meyers, J.P., Ross, P.N., Gostick, J.T., and Liu, Q. (2011). Redox flow batteries: a review. *J. Appl. Electrochem.* 41, 1137–1164.
28. Arenas, L.F., Ponce de León, C., and Walsh, F.C. (2017). Engineering aspects of the design, construction and performance of modular redox flow batteries for energy storage. *J. Energy Storage* 11, 119–153.
29. Goulet, M.-A., and Aziz, M.J. (2018). Flow battery molecular reactant stability determined by symmetric cell cycling methods. *J. Electrochem. Soc.* 165, A1466–A1477.
30. Hu, B., Luo, J., Hu, M., Yuan, B., and Liu, T.L. (2019). A pH-neutral, metal-free aqueous organic redox flow battery employing an ammonium anthraquinone anolyte. *Angew. Chem. Int. Ed. Engl.* 58, 16629–16636.
31. Goulet, M.A., Tong, L., Pollack, D.A., Tabor, D.P., Odom, S.A., Aspuru-Guzik, A., Kwan, E.E., Gordon, R.G., and Aziz, M.J. (2019). Extending the lifetime of organic flow batteries via redox state management. *J. Am. Chem. Soc.* 141, 8014–8019.
32. McCann, G.M., McDonnell, C.M., Magris, L., and More O'Ferrall, R.A. (2002). Enol-keto tautomerism of 9-anthrol and hydrolysis of its methyl ether. *J. Chem. Soc., Perkin Trans. 2* 2, 784–795.

Chem, Volume 6

Supplemental Information

Extremely Stable Anthraquinone Negolytes

Synthesized from Common Precursors

Min Wu, Yan Jing, Andrew A. Wong, Eric M. Fell, Shijian Jin, Zhijiang Tang, Roy G. Gordon, and Michael J. Aziz

Supporting information

Contents

Chemical synthesis and characterization	2
Chemical stability experiments	10
Cyclic Voltammetry (CV) and Rotating Disk Electrode (RDE) Measurements	11
Solubility tests	12
Thermodynamics of the disproportionation reaction.....	13
Anthrone detection	17

Experimental section:

9,10-dihydroanthracene (97%), 3,3-dimethylacrylic acid (97%), succinic anhydride, hydrazine monohydrate (98%), anhydrous dichloromethane, and diethylene glycol (99%) were purchased from Sigma Aldrich, and anhydrous aluminum chloride (95%) was purchased from Alfa Aesar. All chemicals were used as received.

Chemical synthesis and characterization

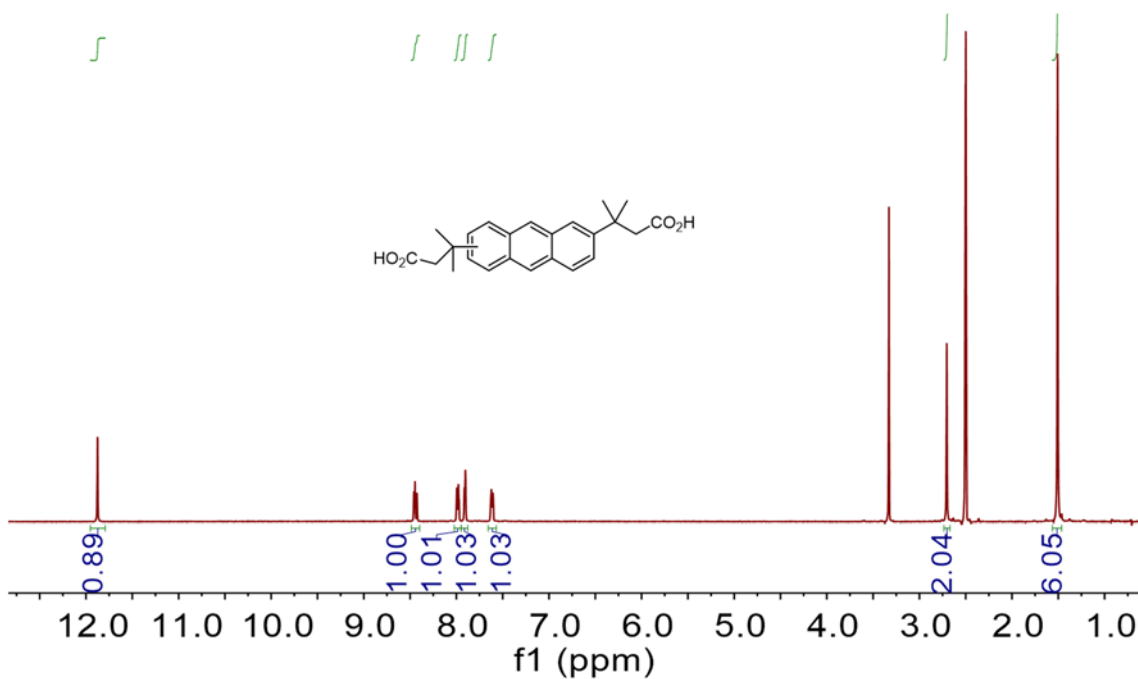


Figure S1. ^1H NMR spectrum of DPivOHAC in $\text{DMSO}-d_6$. Solvent peaks are those that are not integrated. ^1H NMR (500 MHz, $\text{DMSO}-d_6$) δ 11.88 (s, 2H), 8.45 (t, 2H), 7.99 (dd, 2H), 7.91 (d, 2H), 7.62 (d, 2H), 2.71 (s, 2H), 1.51 (s, 6H).

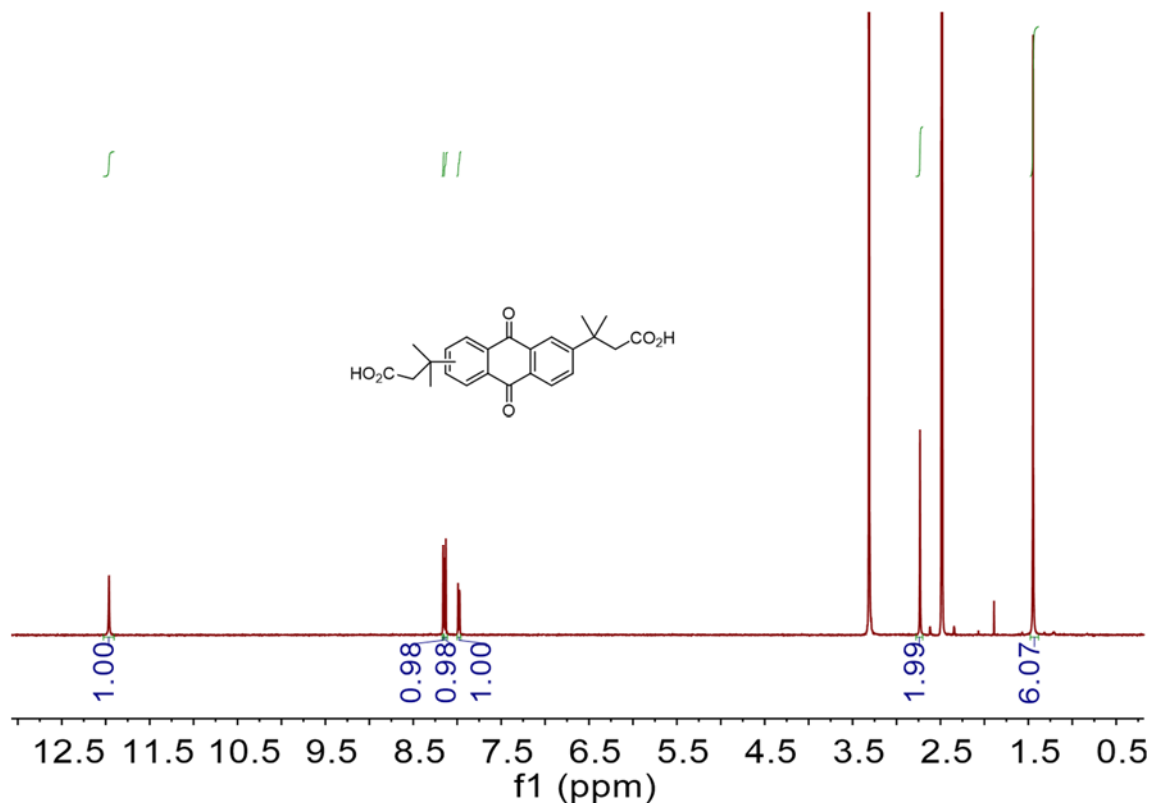


Figure S2. ¹H NMR spectrum of DPivOHAQ in DMSO-*d*₆. Solvent peaks are those that are not integrated. ¹H NMR (500 MHz, DMSO-*d*₆) δ 11.99 (s, 2H), 8.17 (d, 2H), 8.15 (dd, 2H), 8.0 (dd, 2H), 2.75 (s, 2H), 1.46 (s, 6H).

DPivOHAQ synthesized with nitric acid/oxygen method:¹

3 g DPivOHAC (7.94 mmol) was taken in a flask containing 60 mL of acetic acid, refluxed at 95 °C and 12.5 mL of a solution containing concentrated nitric acid (70%), acetic acid and water (1:9:9, by volume) was added dropwise to the well-stirred mixture, while industrial oxygen was bubbled into the solution. The addition took about 10 min, deep-brown fumes evolved. After the reaction was completed (normally within 2 h) the flask was cooled and 1M HCl was added to the solution, and filtrate to get the final DPivOHAQ. Washed with acetone, the final yield is around 80%.

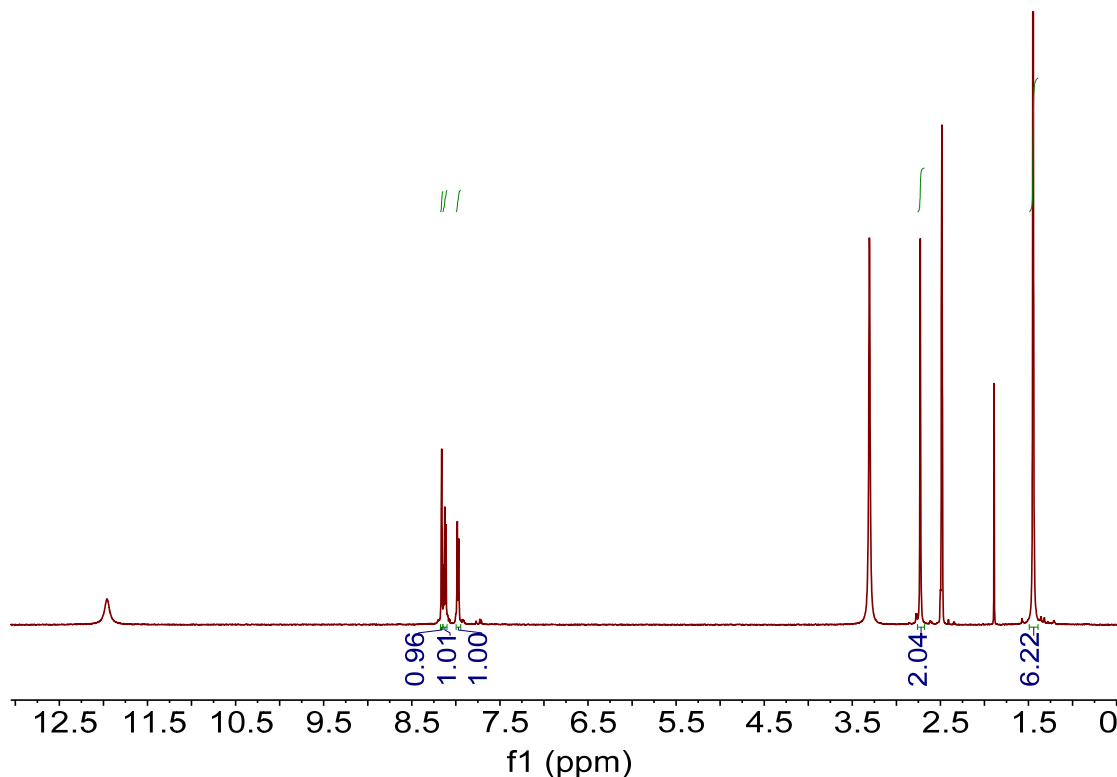


Figure S3. ^1H NMR spectrum of DPivOHAQ synthesized from nitric acid/oxygen method in $\text{DMSO-}d_6$. Solvent peaks (3.3 H_2O , 2.5 DMSO, 1.9 $\text{CH}_3\text{CO}_2\text{H}$) are those that are not integrated. ^1H NMR (500 MHz, $\text{DMSO-}d_6$) δ 11.99 (s, 2H), 8.17 (d, 2H), 8.15 (dd, 2H), 8.0 (dd, 2H), 2.75 (s, 2H), 1.46 (s, 6H).

4,4'-(9,10-dihydroanthracene-diyl)bis(4-oxobutanoic acid) (DOBDHAC):

15.50 g (115.89 mmol) of AlCl_3 was suspended in ~200 mL of anhydrous CH_2Cl_2 . A solution of 5.69 g (56.49 mmol) of succinic anhydride was added and the mixture stirred at 0 °C for 0.5 hour under nitrogen. Subsequently, a solution of 5.00 g (27.74 mmol) of 9,10-dihydroanthracene in ~15 mL of anhydrous CH_2Cl_2 was added to the above mixture and stirred overnight. Then the suspension was filtered to obtain the red solid, which was then washed with ice water twice and filtered to afford a yellow solid (10.5 g). Yield: 99%. ^1H NMR (500 MHz, $\text{DMSO-}d_6$) δ 12.13 (s, 2H), 7.96 (t, 2H), 7.84 (dd, 2H), 7.49 (d, 2H), 4.09 (s, 4H), 3.25 (t, 4H), 2.58 (t, 4H).

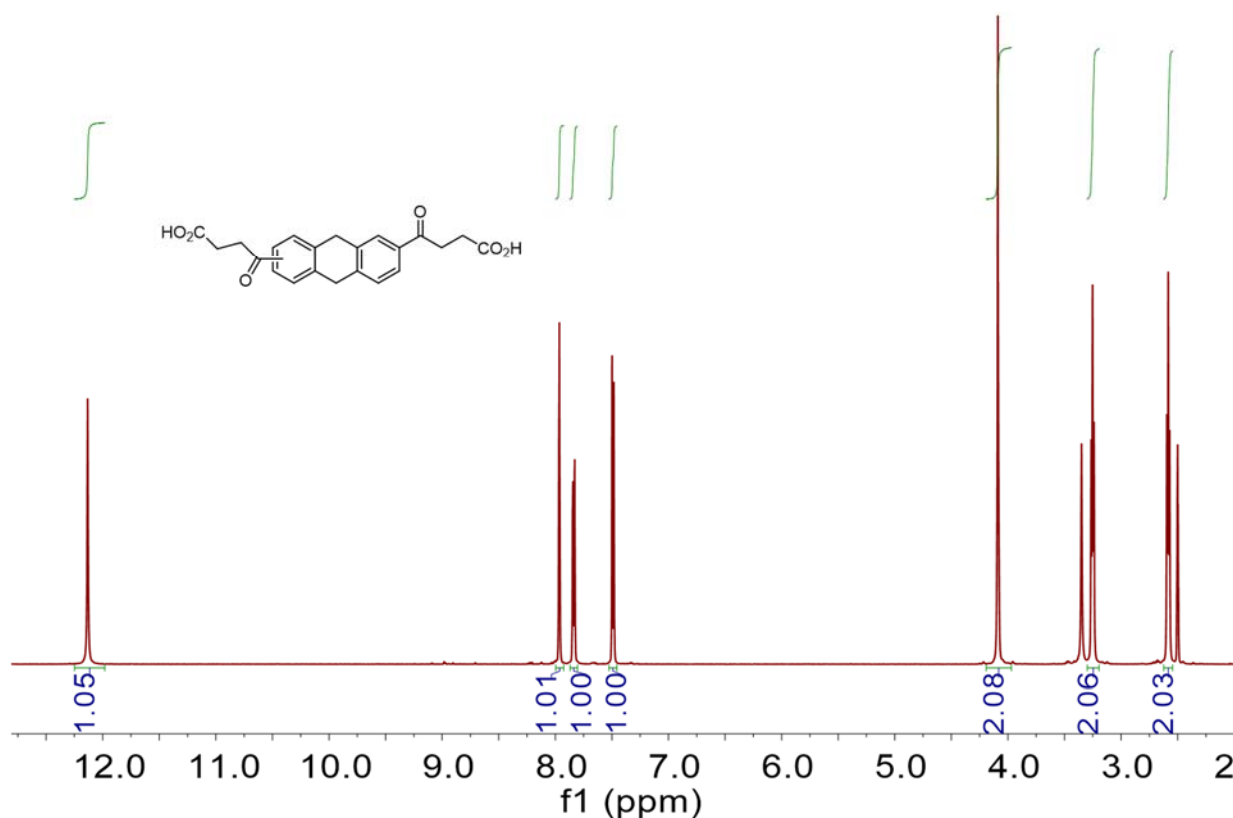


Figure S4. ^1H NMR spectrum of DOBDHAC in $\text{DMSO}-d_6$. Solvent peaks are those that are not integrated.

4,4'-(9,10-dihydroanthracene-diyl)dibutanoic acid (DBDHAC):

To a solution of DOBDHAC (10.5 g, 27.74 mmol) in diethylene glycol (100 mL) at room temperature was added hydrazine monohydrate (98%, 8 mL, 166 mmol). The reaction mixture was stirred for half an hour. Then potassium hydroxide was added (8.73 g, 155.59 mmol) and stirred at 100 °C for 1 hour under nitrogen. Then the temperature was allowed to rise to 200 °C for 4 hours. After cooling to room temperature, 500 mL of water was added to the solution, which was then filtered twice to remove insoluble solid. The filtrate was acidified with 5 M HCl to adjust the pH to 1, and the resulting precipitate was collected and washed with water (500 mL) twice to afford the light brown solid. Yield: approximately 95%. ^1H NMR indicated that the product was DBDHAC (4,4'-(9,10-dihydroanthracene-2,6-diyl)dibutanoic acid) with around 10% percent of DBAC (4,4'-(anthracene-diyl)dibutanoic acid). As both dihydroanthracene and anthracene may be converted to anthraquinone, no further purification was needed at this step. ^1H NMR (500 MHz, $\text{DMSO}-d_6$) DBHAC: δ 7.21 (d, 2H), 7.13 (s, 2H), 6.99 (dd, 2H), 3.83 (t, 4H), 2.55

(t, 4H), 2.20 (t, 4H), 1.78 (m, 4H). DBAC: δ 8.43 (t, 2H), 7.99 (dd, 2H), 7.80 (s, 2H), 7.37 (t, 2H), 2.79 (t, 4H), 2.29 (t, 4H), 1.93 (m, 4H).

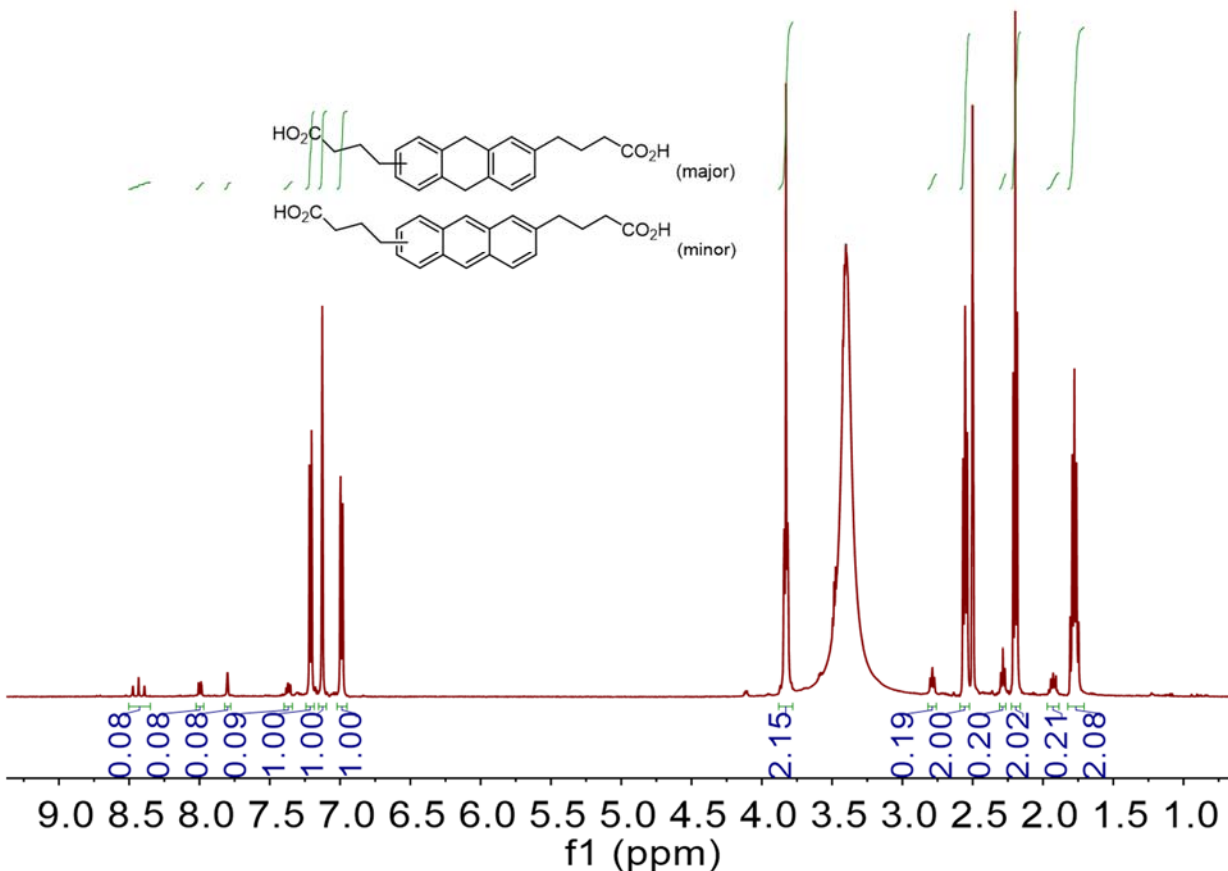


Figure S5. ^1H NMR spectrum of DBDHAC in $\text{DMSO-}d_6$. Solvent peaks are those that are not integrated.

4,4'-(9,10-anthraquinone-diyl)dibutanoic acid (DBAQ):

DBDHAC (10 g, 28.4 mM) was dissolved in 100 mL glacial acetic acid. Then, a CrO_3 solution, prepared by dissolving CrO_3 (7.1 g, 71 mM) in 4 mL of water, was added to the above solution. The reaction mixture was allowed to stir at room temperature overnight. Then 300 mL of water was added to the mixture, which was then filtered to afford the yellow product. The product was dissolved in base and further acidified to afford the yellow precipitate. The last step is used to remove the residual Cr (III) compound. Yield: 90%. ^1H NMR (500 MHz, $\text{DMSO-}d_6$) δ 8.05 (dd, 2H), 7.94 (t, 2H), 7.70 (dd, 2H), 2.77 (t, 4H), 2.27 (t, 4H), 1.86 (m, 4H).

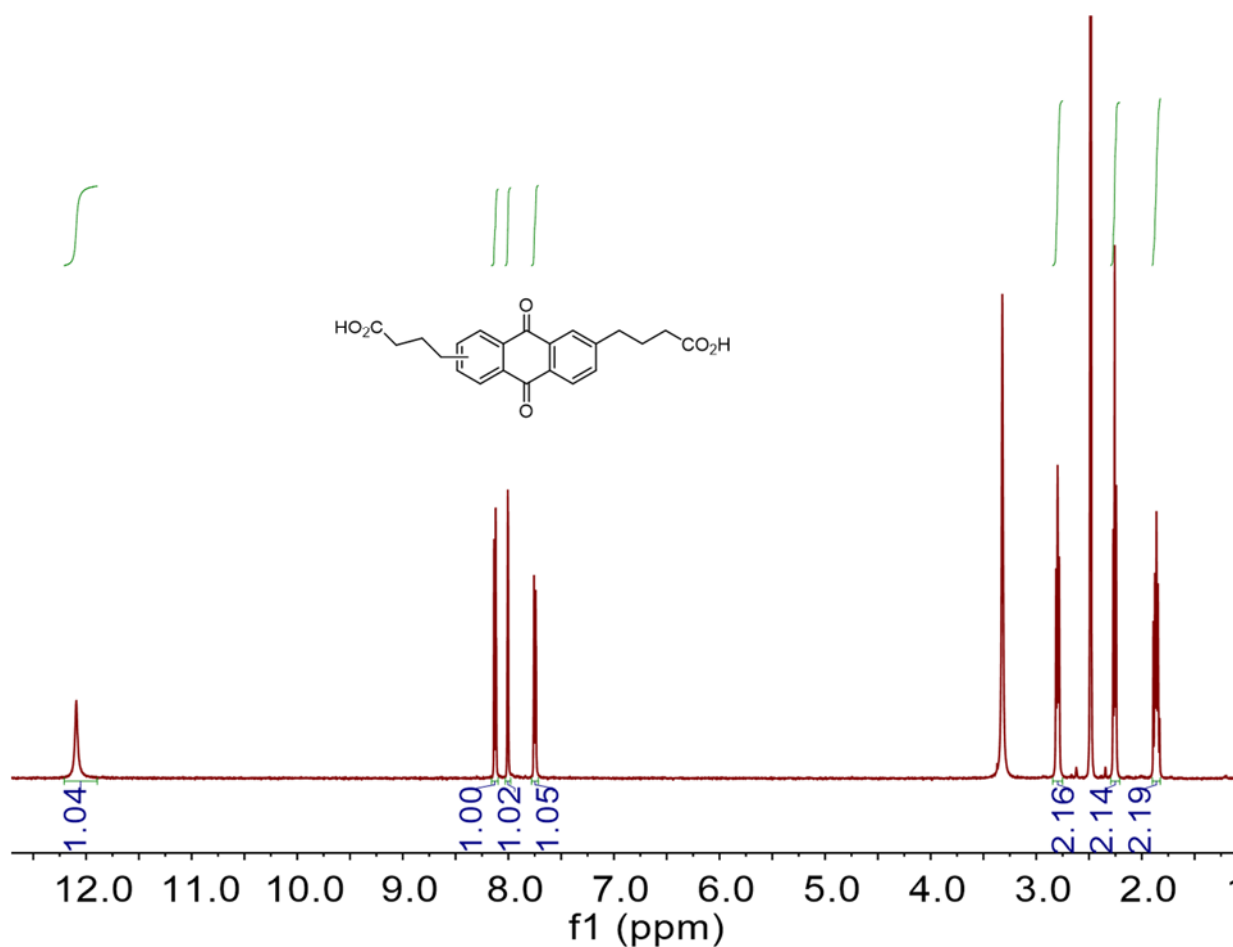


Figure S6. ¹H NMR spectrum of DBAQ in DMSO-*d*₆. Solvent peaks are those that are not integrated.

DBAQ synthesized with the nitric acid/oxygen method:¹

3 g DBDHAC (8.52 mmol) was taken in a flask containing 60 mL of acetic acid, refluxed at 95 °C and 13.5 mL of a solution containing concentrated nitric acid (70%), acetic acid and water (1:9:9, by volume) was added dropwise to the well-stirred mixture, while industrial oxygen was bubbled into the solution. The addition took about 10 min, deep-brown fumes evolved. After the reaction was completed (normally within 2 h) the flask was cooled and 1M HCl was added to the solution, and filtrate to get the final DBAQ. Yield: 97%.

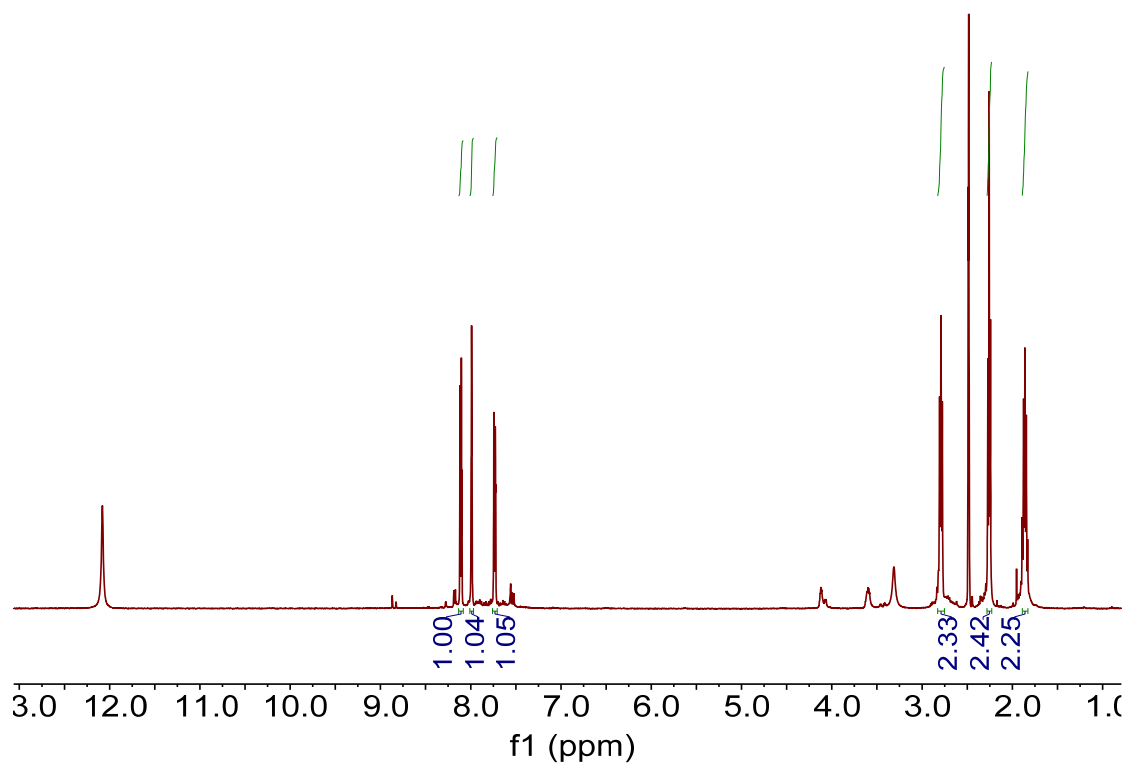
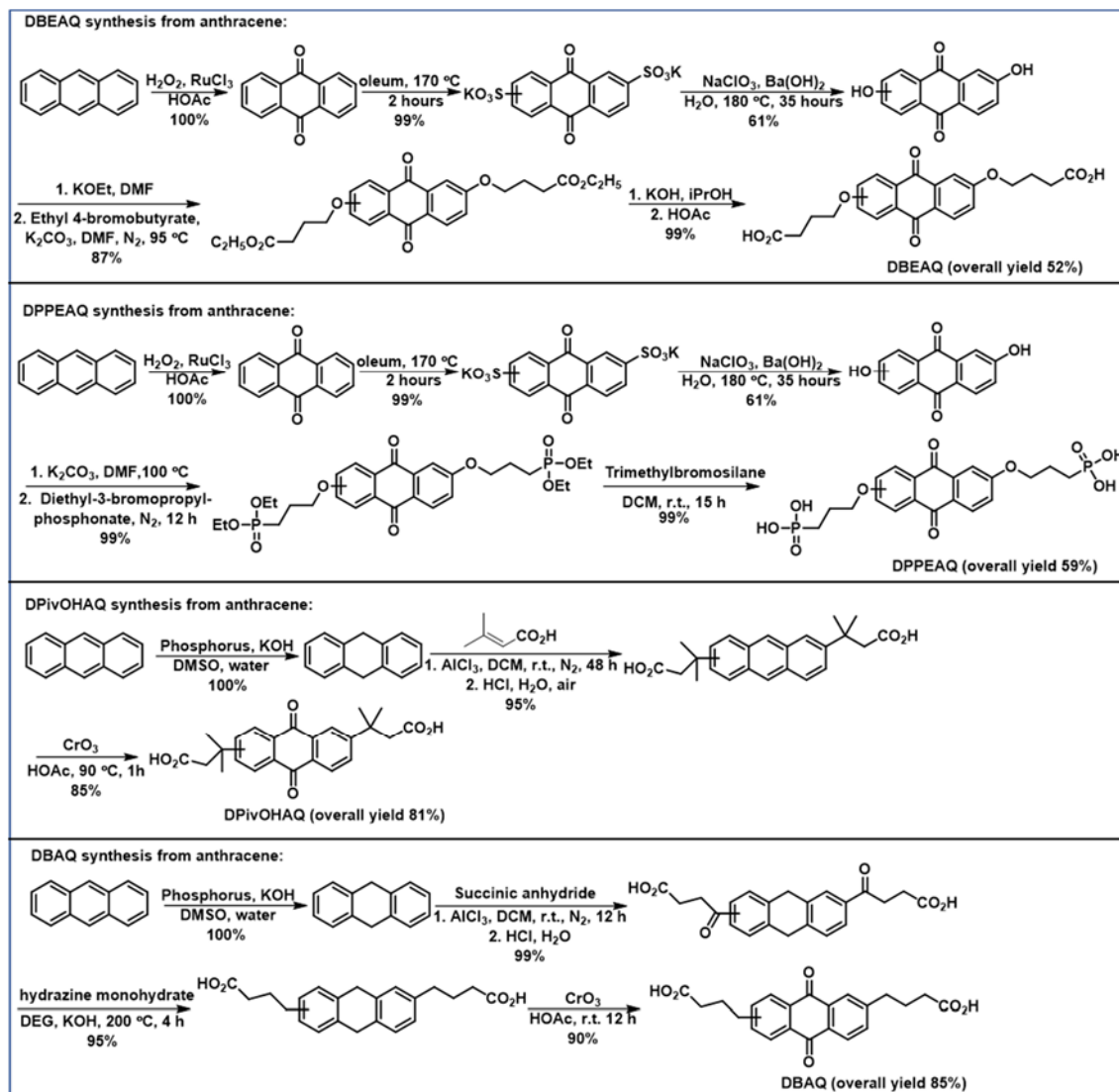


Figure S7. ^1H NMR spectrum of DBAQ synthesized from the nitric acid/oxygen method in $\text{DMSO-}d_6$. Solvent peaks (3.3 H_2O , 2.5 DMSO) and small impurities are those that are not integrated. ^1H NMR (500 MHz, $\text{DMSO-}d_6$) δ 8.05 (dd, 2H), 7.94 (t, 2H), 7.70 (dd, 2H), 2.77 (t, 4H), 2.27 (t, 4H), 1.86 (m, 4H).

Note that the reaction condition is not optimized, and the impurities in the final compound is consider to come from the anthracene core rather than from the functionalized chain.

Comparison of synthetic conditions for DPivOHAQ, DBAQ, DBEAQ, and DPPEAQ



Scheme S1. Comparison of the synthetic routes for DBEAQ,²⁻⁵ DPPEAQ,^{2-4,6} DPivOHAQ,⁷ and DBAQ⁷ from anthracene.

Table S1. Lab-scale cost for the side chain resources and starting materials of four stable anthraquinones from Sigma-Aldrich in Nov. 2019.

	2,6-DHAQ	DBEAQ	DPPEAQ	9,10-dihydroanthracene	DPivOHAQ	DBAQ
side chain		ethyl 4-bromobutyrate	diethyl-3-bromopropylphosphonate		3,3-dimethylacrylic acid	succinic anhydride
cost	5 g: \$105	250 g: \$138	5mL: \$91	5 g: \$41.1	500 g: \$152	500 g: \$41
unit price (\$/mol)	5044.4	107.7	3498	1481	30.4	8.2

Note that even though the lab-scale cost of 2,6-DHAQ is high, the mass production cost of 2,6-DHAQ is predicted to be as low as \$2.4/kg by Borealis Technology Solutions

LLC.⁸ As the lab-scale cost of 9,10-dihydroanthracene is approximately one third of that of 2,6-DHAQ, we suppose the cost of 9,10-dihydroanthracene could be inexpensive if produced in large-scale.

Chemical stability experiments

Samples of DPivOHAQ at 0.1 M concentration and at pH 14 were stored in fluorinated ethylene propylene bottles and heated in an oven at 65 °C for 8 days. The extent of decomposition was determined by ¹H NMR, with peak integrals measured relative to an internal standard of NaCH₃SO₃ prepared at 10 mM concentration in D₂O. All samples were diluted in this deuterated solvent containing the internal standard at a fixed ratio of 1:5.

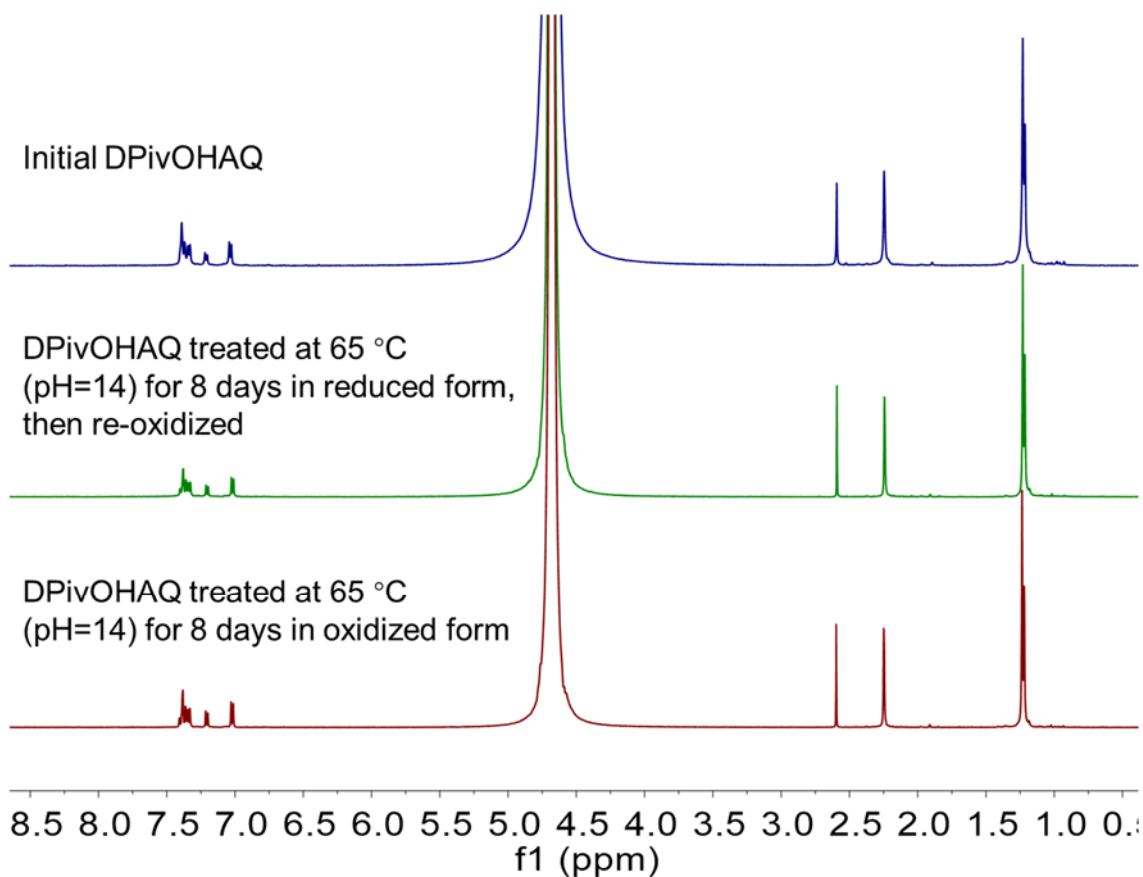


Figure S8. ¹H NMR spectra (500 MHz, 1 M KOD in D₂O with 10 mM NaCH₃SO₃ internal standard) of (a) the oxidized form of DPivOHAQ in pH 14 aqueous solution (1 M KOH); (b) DPivOHAQ treated at 65 °C for 8 days at 0.1 M concentration in pH 14 aqueous solution (1 M KOH) in the reduced form and then re-oxidized in order to compare to samples tested in the oxidized form; (c) DPivOHAQ treated at 65 °C for 8 days at 0.1 M concentration in pH 14

aqueous solution (1 M KOH) in the oxidized form. No apparent decomposition was detected; the integration did not appreciably change.

Cyclic Voltammetry (CV) and Rotating Disk Electrode (RDE) Measurements

Glassy carbon was used as the working electrode for all three-electrode CV tests. RDE experiments were conducted using a Pine Instruments Modulated Speed Rotator AFMSRCE equipped with a 5 mm diameter glassy carbon working electrode, a Ag/AgCl reference electrode (BASi, pre-soaked in a 3 M NaCl solution), and a graphite counter electrode. The diffusion coefficient of the oxidized form of DPivOHAQ was calculated using the Levich equation, which relates the mass-transport-limited current to the number of electrons transferred (n), the area of the electrode (A), and the concentration of redox-active species in the electrolyte (C) by plotting the mass-transport-limited current against the square root of the rotation rate (Figure S9b) with the following parameters: $n = 2$, $F = 96,485$ Coulombs/mol, $A = 0.196$ cm², $C = 5$ mM, kinematic viscosity of 1 M KCl = 0.89×10^{-6} m²/s.⁹ The resulting value of the diffusion coefficient for the oxidized form of DPivOHAQ is 2.4×10^{-6} cm²/s.

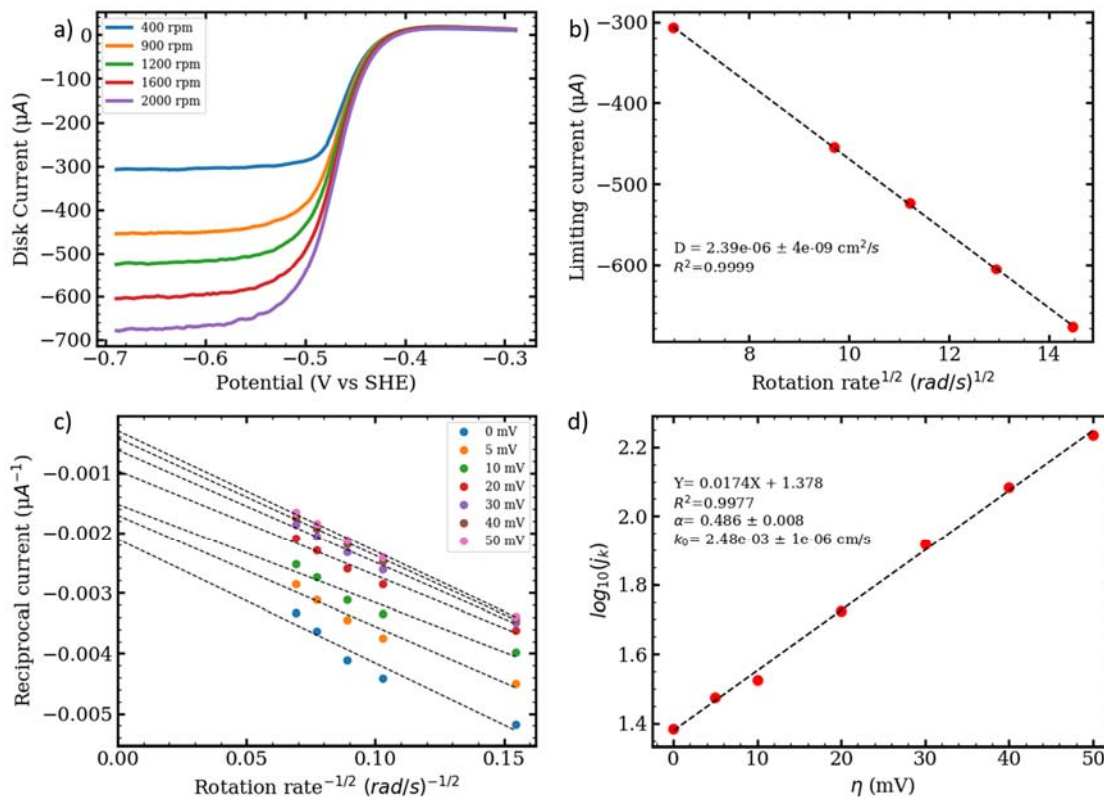


Figure S9. DPivOHAQ reduction kinetics in RDE. a) Linear sweep voltammograms of 5 mM DPivOHAQ in 1 M KCl at pH 12 on a glassy carbon electrode at rotation rates between 400 and

2000 rpm. b) Levich plot (limiting current versus square root of rotation rate in rad/s) of 5 mM DPivOHAQ in 1 M KCl at pH 12. Limiting current is taken as the current at -0.65 V in (a). The slope yields a diffusion coefficient for the oxidized form of DPivOHAQ of $2.39 \times 10^{-6} \text{ cm}^2 \text{ s}^{-1}$. c) Koutecky-Levich plot (reciprocal current versus inverse square root of rotation rate in rad/s) of 5 mM DPivOHAQ in 1 M KCl at pH12. d) Fitted Tafel plot of 5 mM DPivOHAQ in 1 M KCl at pH 12. The charge transfer coefficient is calculated to be 0.49, and the rate constant is calculated to be $2.48 \times 10^{-3} \text{ cm s}^{-1}$.

Solubility tests

For the solubility of K₂DBAQ, we prepared a 1.0 M solution in pH 12 KOH and found that it remained fully dissolved. We did not determine an upper limit. Therefore we report the solubility as 1.0 M.

The solubility limit of DPivOHAQ was measured in the oxidized form by adding the potassium salt of DPivOHAQ (prepared by reacting DPivOHAQ with potassium hydroxide in water) until no further solid could be dissolved. The mixture was adjusted to pH 12. After the suspension was filtered through a nylon 0.45 μm syringe filter, a saturated solution of DPivOHAQ at pH 12 was obtained. The saturated solution was then diluted 20,000 times while maintaining a pH of 12, and the concentration was evaluated by UV-Vis spectrophotometry (Agilent Cary 60 spectrophotometer). The concentration was calculated according to a pre-calibrated absorbance concentration curve of known concentrations of DPivOHAQ at pH 12. The resulting value of the solubility of the oxidized form of DPivOHAQ at pH 12 is 0.74 M.

Solubility of the oxygen-sensitive reduced form of DPivOHAQ was not measured, but was expected to be higher than the oxidized form because: (1) no precipitation was observed after full electrochemical reduction of DPivOHAQ; (2) we expect the two extra negative charges on the reduced form to make quinone-quinone interactions unfavorable and increase its solubility;¹⁰ and (3) anthraquinone is known to be insoluble in base, whereas the reduced form of anthraquinone is readily dissolved in alkaline solution and is often called soluble anthraquinone.¹¹

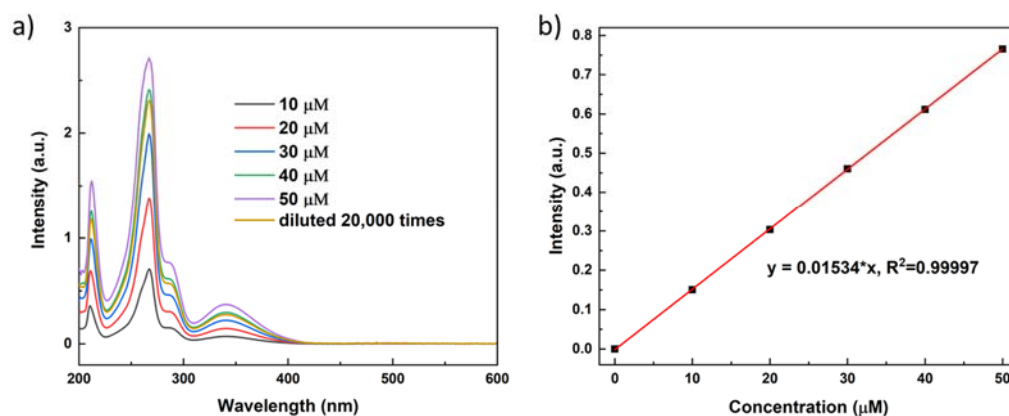
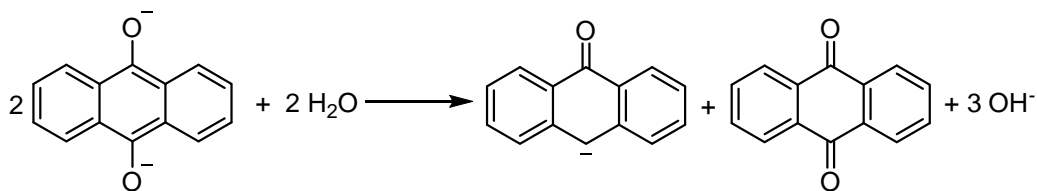


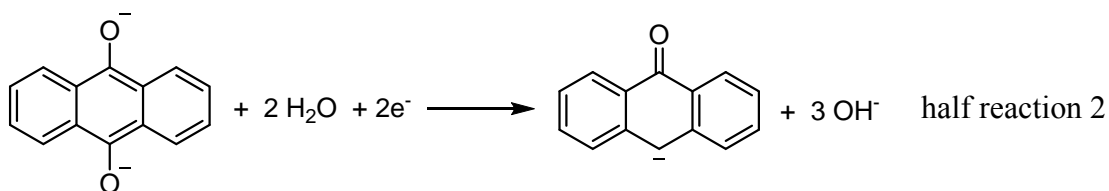
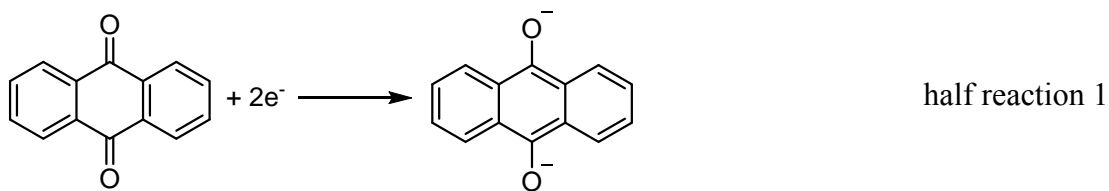
Figure S10. a) UV–Vis spectra of DPivOHAQ at different concentrations; b) the absorbance at 287.9 nm versus the concentration; a least-squares linear fit to the data was performed to generate the calibration curve utilized in this work. The saturated sample was diluted 20,000 times and calculated to be 0.74 M at pH 12.

Thermodynamics of the disproportionation reaction

When the pH is between 12 and 14, both 9,10-dihydroxyanthracene (reduced anthraquinone) and anthrone ($pK_a = 10$)¹² are deprotonated, and the disproportionation reaction proceeds as follows:



This disproportionation reaction is a combination of the following two half reactions:



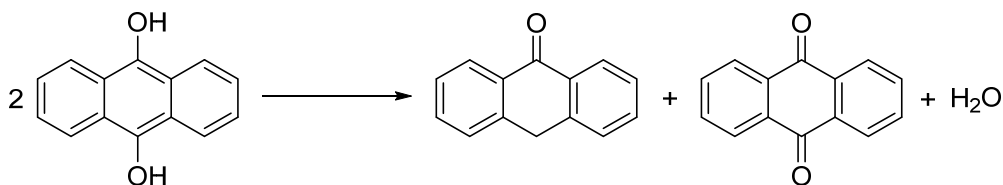
Within this pH range, the redox potential E_1 for half reaction 1 is pH independent, whereas the redox potential E_2 for the half reaction 2 decreases by approximately 89 mV per pH unit increase based on Nernst equation. The Gibbs free energy change ΔG per molecule of anthrone formed by the disproportionation reaction (half reaction 2 minus half reaction 1) is given by:

$$\Delta G = -2 \times F \times (E_2 - E_1) / N_A$$

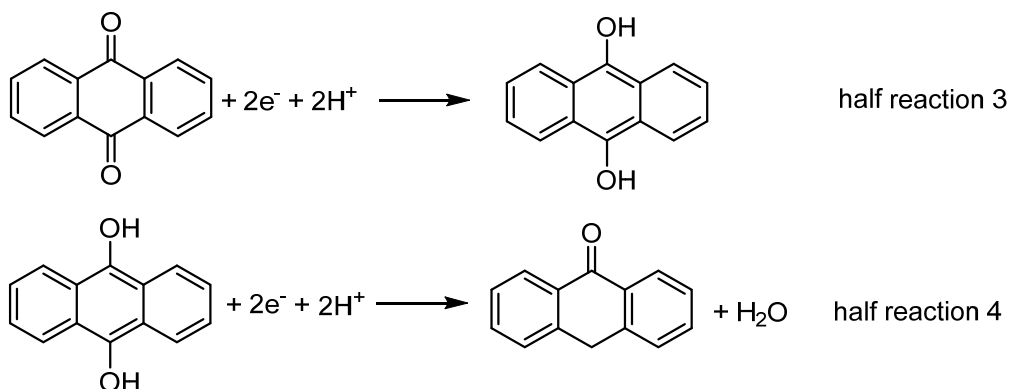
assuming reactants and products (other than OH^-) have unit activities and the activity of OH^- is consistent with the pH.

As pH increases, the Gibbs free energy change ΔG increases, and the disproportionation reaction is less prone to happen. This observation is equivalent to the statement that the overall reaction within this pH range involves OH^- , so the activity of OH^- factors into the reaction quotient and equilibrium constant. By Le Chatelier's principle, the reaction will be disfavored as the pH increases.

When the pH is below the $\text{p}K_{a1}$ (typically approximately 7) of 9,10-dihydroxyanthracene, the disproportionation reaction becomes:



The two corresponding two half reactions are



The redox potential E_3 for half reaction 3 decreases by approximately 59 mV per pH unit increase based on Nernst equation, and so does the redox potential E_4 .

The Gibbs free energy change $\Delta G'$ per molecule of anthrone formed by the disproportionation reaction (half reaction 4 minus half reaction 3) is given by:

$$\Delta G' = -2 \times F \times (E_4 - E_3) / N_A$$

assuming reactants and products (other than H^+) have unit activities and the activity of H^+ is consistent with the pH.

As pH (below pK_{a1}) increases, the Gibbs free energy change $\Delta G'$ is constant. This observation is equivalent to the statement that the overall reaction within this pH range does not involve H^+ , so the activity of H^+ does not factor into the reaction quotient and equilibrium constant.

If we draw a theoretical Pourbaix diagram for the two half reactions of the anthrone-forming disproportionation reaction according to Nernst equation (assuming that the pK_a of anthrone lies between the pK_{a1} and pK_{a2} of hydroquinone), we obtain:

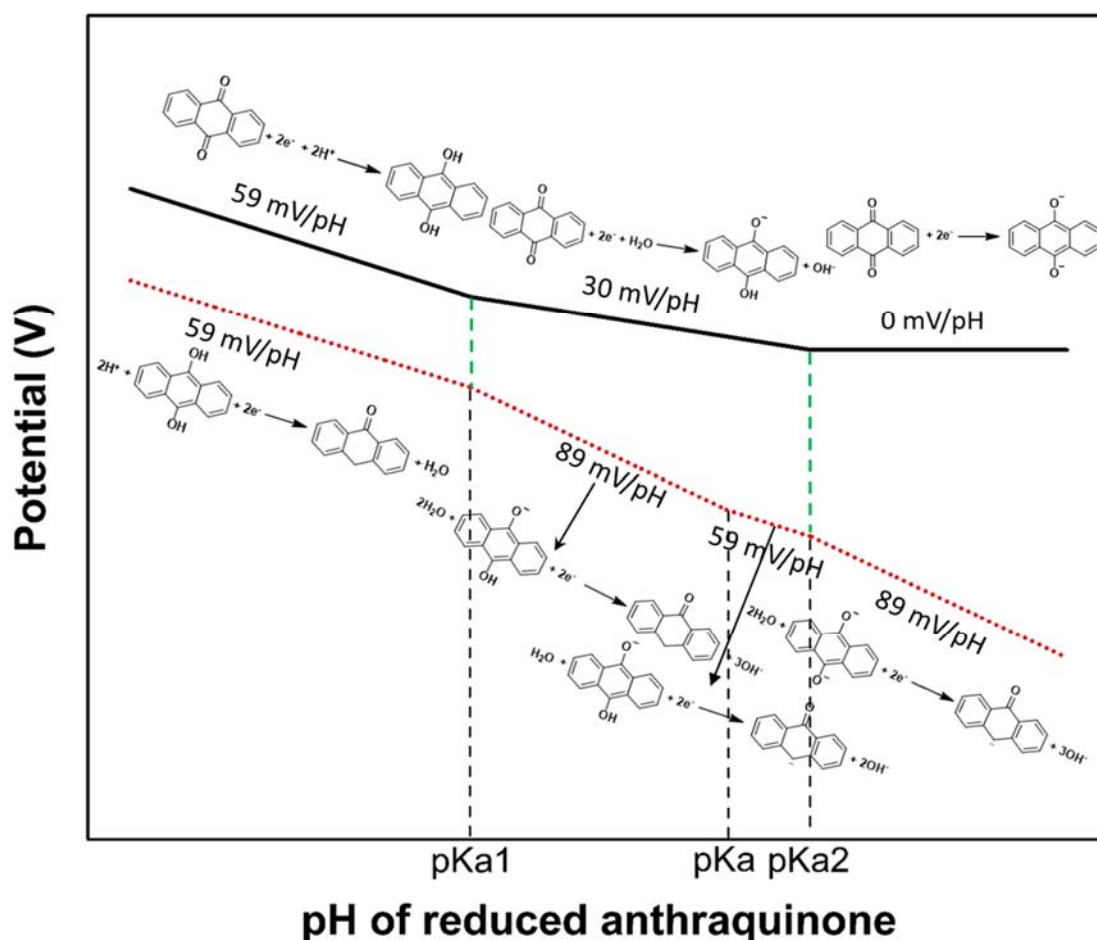


Figure S11. Representative Pourbaix diagram of anthraquinone, anthrahydroquinone, and anthrone. The pK_{a1} and pK_{a2} belong to the 9,10-dihydroxyanthracene (anthrahydroquinone). The pK_a (reported to be approximately 10) belongs to anthrone.¹² Here we assume that the pK_a of anthrone lies between the pK_{a1} and pK_{a2} of anthrahydroquinone.

This Pourbaix diagram illustrates that the Gibbs free energy change ΔG for the disproportionation reaction is larger at alkaline pH than at neutral or acidic pH. Therefore, anthrone formation is disfavored at alkaline pH relative to neutral or acidic pH. In real applications with a reasonable concentration of quinone, even starting at pH 7, the pH will increase to (or above) the pK_{a2} of 9,10-dihydroxyanthraquinone upon quinone reduction; therefore, it is still possible to get a relatively stable anthraquinone negolyte starting at pH 7.

Anthrone detection

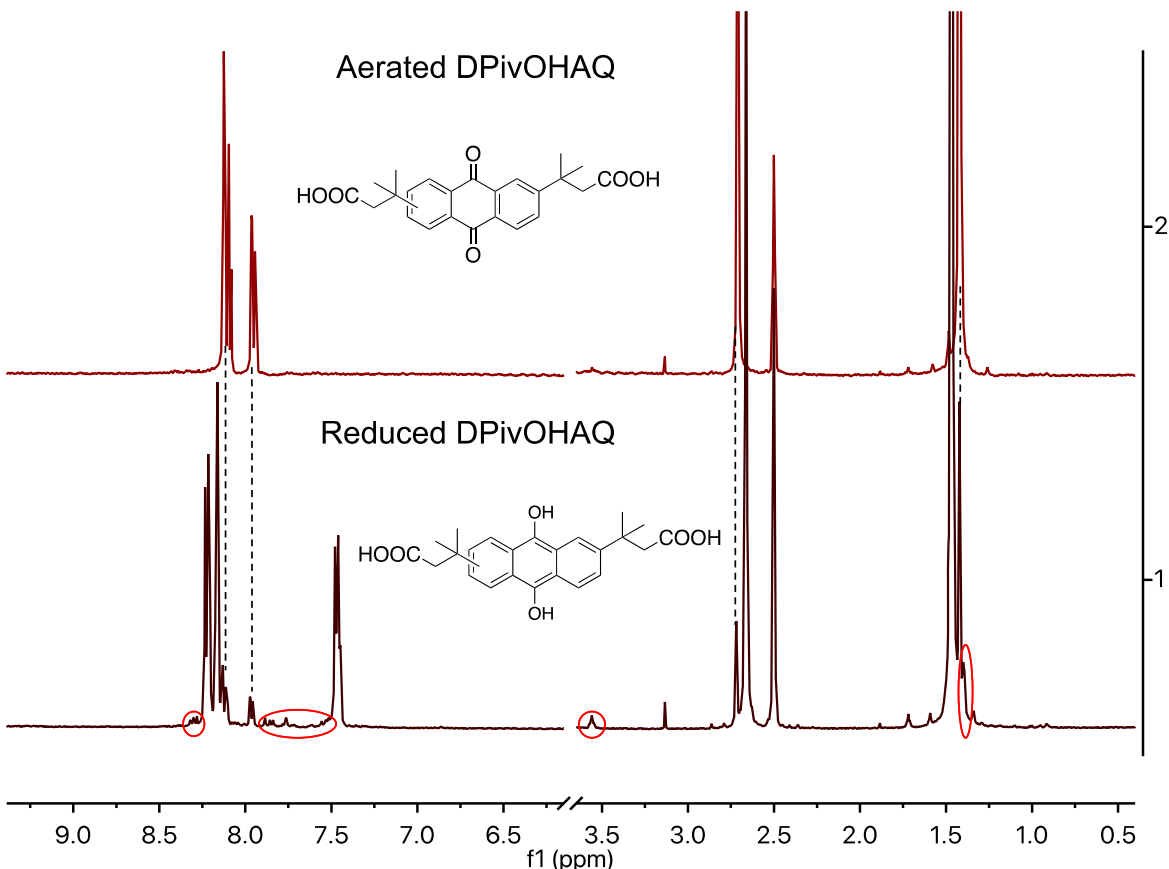


Figure S12. ^1H NMR spectra of the reduced and aerated DPivOHAQ in $\text{DMSO-}d_6$. Sample preparation: 5 mL of 0.1 M DPivOHAQ was fully charged to $\sim 100\%$ SOC and stored in a brown vial in a glovebox for 238 days. After that, an aliquot was taken and acidified with concentrated HCl to obtain the protonated and reduced DPivOHAQ precipitate after clear solution was removed. The protonated and reduced DPivOHAQ was re-dissolved in $\text{DMSO-}d_6$ and stored in a J. Young NMR tube for ^1H NMR spectrometry. The aerated sample was prepared by exposing the same reduced sample to air and shaking the NMR tube for several minutes before collecting the NMR spectrum. The ^1H NMR spectrum of the reduced sample revealed, in addition to peaks from reduced DPivOHAQ and a small amount of the oxidized form, some appreciable peaks highlighted with red circles, corresponding to signals from unknown compounds. However, these signals disappeared when the same NMR sample was aerated, indicating that the unknown compounds can either be oxidized back to DPivOHAQ or convert into other products with no observable signals above the detection limit of the NMR instrument.

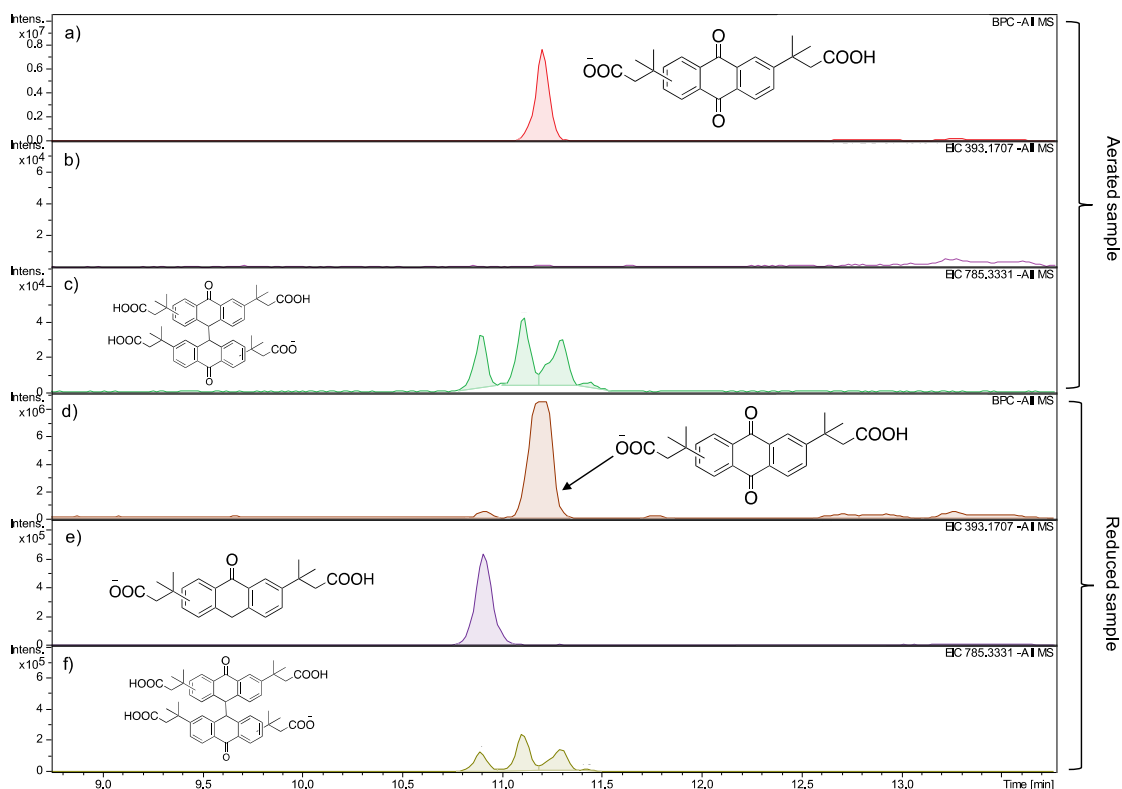


Figure S13. LC-MS results from the reduced DPivOHAQ samples stored for 238 days. a) The base peak chromatogram of the aerated sample. b) The extracted-ion chromatogram for the anthrone derivative from the aerated sample. c) The extracted-ion chromatogram for the anthrone dimer derivative from the aerated sample. d) The base peak chromatogram of the reduced sample. e) The extracted-ion chromatogram for the anthrone derivative from the reduced sample. f) The extracted-ion chromatogram for the anthrone dimer derivative from the reduced sample. In the reduced sample, both anthrone and anthrone dimer forms were detected. After aeration, no anthrone form is detected. The anthrone dimer accounts for 1.24% in the aerated sample, corresponding a fade rate of 1.90% per year for the reduced DPivOHAQ after aeration. Sample preparation: 5 mL of 0.1 M DPivOHAQ was fully charged to ~100% SOC and stored in a brown vial in a glovebox for 238 days. After that, aliquots were taken and acidified with concentrated HCl to obtain protonated DPivOHAQ precipitate after clear solution was removed. The protonated and reduced DPivOHAQ was re-dissolved in DMSO. The resulting solution was further diluted to the desired concentration (10-20 μ M) by acetonitrile/water co-solvents (V/V=1:1). One sample was stored in a glovebox in the reduced form prior to the LC-MS measurement, whereas another sample was intentionally aerated. After that, the two samples were immediately subjected to the LC-MS experiment.

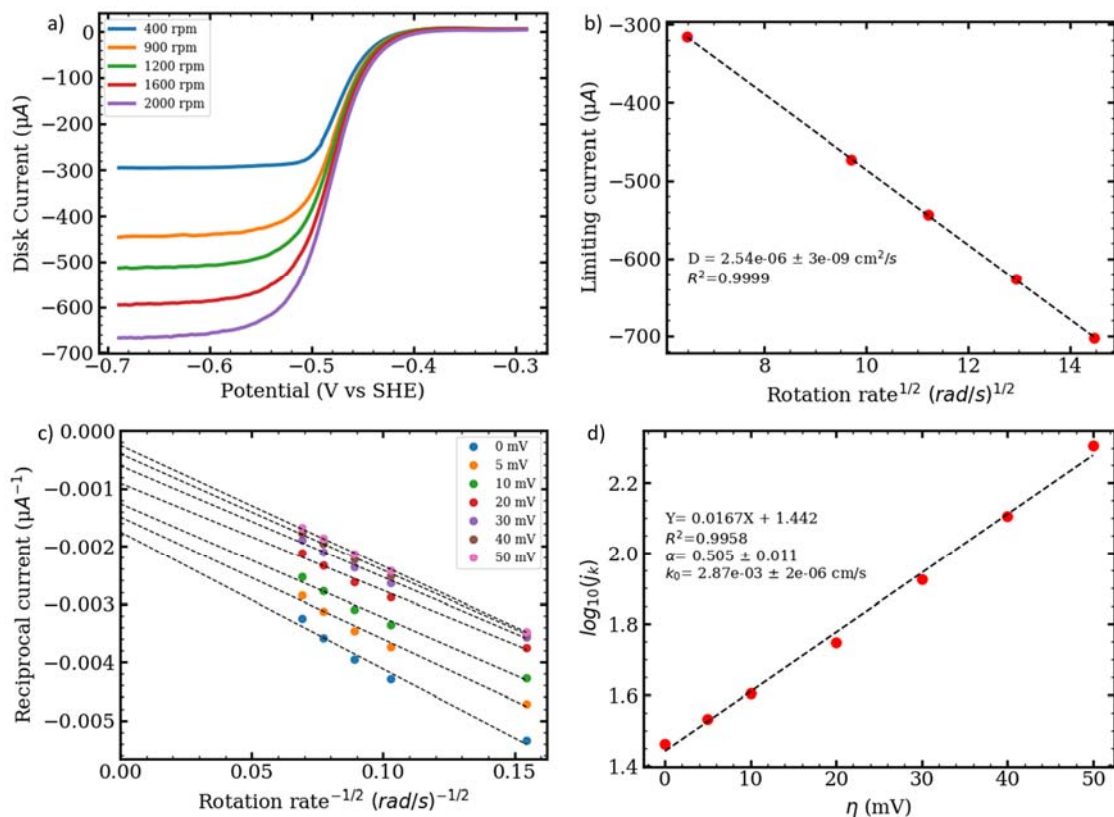


Figure S14. RDE test for DBAQ. a) Linear sweep voltammograms of 5 mM DBAQ in 1 M KCl at pH 12 on a glassy carbon electrode at rotation rates between 400 and 2000 rpm. b) Levich plot (limiting current versus square root of rotation rate in rad/s) of 5 mM DBAQ in 1 M KCl at pH 12. Limiting current is taken as the current at -0.65 V in (a). The slope yields a diffusion coefficient for the oxidized form of DBAQ of $2.54 \times 10^{-6} \text{ cm}^2 \text{ s}^{-1}$. c) Koutecky-Levich plot (reciprocal current versus inverse square root of rotation rate in rad/s) of 5 mM DBAQ in 1 M KCl at pH 12. d) Fitted Tafel plot of 5 mM DBAQ in 1 M KCl at pH 12. The charge transfer coefficient is calculated to be 0.50, and the rate constant is calculated to be $2.87 \times 10^{-3} \text{ cm s}^{-1}$.

References

1. Das, C. K.; Das, N. S. Oxidation of Anthracene to Anthraquinone in Liquid-Phase with an Air/Oxygen/Nitric Acid System. *J. Chem. Tech. Bioiechnol.* **1982**, 32, 643-649.
2. Tandon, P. K.; Baboo, R.; Singh, A. K. Simple and economical conversion of organic compounds with H₂O₂ catalyzed by ruthenium (III) chloride. *Appl. Organometal. Chem.* **2006**, 20 (1), 20.
3. Huskinson, B.; Marshak, M. P.; Suh, C.; Er, S.; Gerhardt, M. R.; Galvin, C. J.; Chen, X.; Aspuru-Guzik, A.; Gordon, R. G.; Aziz, M. J. A metal-free organic-inorganic aqueous flow battery. *Nature* **2014**, 505 (7482), 195.
4. Hall, J.; Perkin, A. G. Reduction products of the hydroxyanthraquinones. Part II. *J. Chem. Soc., Trans.* **1923**, 123, 2029.
5. Kwabi, D. G.; Lin, K.; Ji, Y.; Kerr, E. F.; Goulet, M.-A.; De Porcellinis, D.; Tabor, D. P.; Pollack, D. A.; Aspuru-Guzik, A.; Gordon, R. G.; Aziz, M. J. Alkaline quinone flow battery with long lifetime at pH 12. *Joule* **2018**, 2 (9), 1894.
6. Ji, Y.; Goulet, M.-A.; Pollack, D. A.; Kwabi, D. G.; Jin, S.; Porcellinis, D.; Kerr, E. F.; Gordon, R. G.; Aziz, M. J. A phosphonate-functionalized quinone redox flow battery at near-neutral pH with record capacity retention rate. *Adv. Energy Mater.* **2019**, 9 (12), 1900039.
7. Kuimov, V. A.; Gusarova, N. K.; Malysheva, S. F.; Trofimov, B. A. Transition metal-free regioselective access to 9,10-dihydroanthracenes via the reaction of anthracenes with elemental phosphorus in the KOH/DMSO system. *Tetrahedron Lett.* **2018**, 59 (52), 4533.
8. Yang, Z.; Tong, L.; Tabor, D. P.; Beh, E. S.; Goulet, M.-A.; De Porcellinis, D.; Aspuru-Guzik, A.; Gordon, R. G.; Aziz, M. J. Alkaline benzoquinone aqueous flow battery for large-scale storage of electrical energy. *Adv. Energy Mater.* **2018**, 8 (8), 1702056.
9. Kestin, J.; Khalifa, H. E.; Correia, R. J. Tables of the dynamic and kinematic viscosity of aqueous KCl solutions in the temperature range 25–150 °C and the pressure range 0.1–35 MPa. *J. Phys. Chem. Ref. Data* **1981**, 10 (1), 57.
10. Karandur, D.; Wong, K.-Y.; Pettitt, B. M. Solubility and Aggregation of Gly5 in Water. *J. Phys. Chem. B* **2014**, 118 (32), 9565-9572.
11. Smith, P.; Tatchell, A. R. *Aromatic Chemistry: Organic Chemistry for General Degree Students*. Elsevier: 2016, p196-221.
12. McCann, G. M.; McDonnell, C. M.; Magris, L.; More O'Ferrall, R. A. Enol–keto tautomerism of 9-anthrol and hydrolysis of its methyl ether. *J. Chem. Soc., Perkin Trans.* **2002**, 2 (4), 784.